Pore-scale mechanisms underlying the behavior of enhanced bentonites exposed to aggressive inorganic solutions

Applied Clay Science 251 (2024) 107318

Contents lists available at ScienceDirect

Applied Clay Science

journal homepage: www.elsevier.com/locate/clay

Review article

Pore-scale mechanisms underlying the behavior of enhanced bentonites exposed to aggressive inorganic solutions

Nicolò Guarena *, Andrea Dominijanni, Mario Manassero

Department of Structural, Geotechnical and Building Engineering, Polytechnic University of Turin, corso Duca degli Abruzzi 24, 10129 Turin, Italy

ARTICLE INFO

Keywords:
Bentonite fabric
Chemical compatibility
Hydraulic conductivity
Osmotic swelling
Polymer amendment
Semipermeable membrane behavior

ABSTRACT

Understanding the mechanisms that control the hydraulic and semipermeable membrane behavior of enhanced bentonites (EBs), which comprise natural montmorillonite amended with polymers or organic compounds, is important for assessing the long-term performance of engineered barriers manufactured from these materials. Accordingly, the available experimental evidence for the hydraulic and semipermeable membrane behavior of EBs was critically interpreted through a theoretical framework, which allows the macroscopic transport and swelling properties of chemically active clays to be related to a limited number of intrinsic, state, and fabric parameters. Four commonly evaluated EBs were interpreted, namely, Multiswellable Bentonites (MSBs), Dense Prehydrated GCLs (DPH-GCLs), HYPER Clays (HCs), and Bentonite Polymer Composites (BPCs). Osmotic swelling, which is the primary mechanism for significant swelling and low hydraulic conductivity of unenhanced (natural) sodium bentonite, is not significantly influenced by polymer amendment. The primary mechanism controlling the conductive porosity and the flow path tortuosity upon permeation of BPCs with concentrated electrolyte solutions is intergranular pore clogging by sodium polyacrylate, whereas the mechanism for the same behavior of DPH-GCLs and, probably to a lesser extent, of HCs is preservation of a dispersed clay fabric via intercalation of sodium carboxymethyl cellulose between the montmorillonite unit layers. Similar to BPCs, direct exposure of MSBs to liquids with aggressive chemistries induces the fabric to flocculate to a greater extent than that of prehydrated natural bentonites. However, unlike BPCs, the decrease in the conductive porosity of MSBs is due to a greater compressibility of the solid skeleton rather than to a pore-clogging mechanism.

1. Introduction

Engineered bentonite-based barriers are increasingly being accepted as replacements for traditional pollutant containment systems over a wide range of geoenvironmental applications, such as in landfill bottom liners and cover systems that include geosynthetic clay liners (GCLs) or bentonite-amended soil liners (Rowe, 1998, 2014; Manassero et al., 2000; Bouazza, 2002), cement-bentonite or soil-bentonite vertical cutoff walls for remediation of contaminated sites (Brandl, 1994; Manassero et al., 1995; Soga et al., 2013), and compacted bentonite buffers used to isolate canisters containing high level radioactive waste for deep geological disposal (Komine and Ogata, 1999; Bourg et al., 2003; Gens et al., 2009; Villar et al., 2020). The primary reasons justifying the use of natural bentonites (NBs) in place of alternative materials for these barriers are a low hydraulic conductivity, k (typically $\leq 10^{-11}$ m·s^{-1}), upon permeation with low ionic strength aqueous solutions (e.g. Puma et al., 2015), the ability to accommodate large differential settlements without cracking, a self-healing capacity when subjected to punctures during handling and installation, and the ability to exhibit semipermeable membrane behavior (Manassero and Dominijanni, 2003; Shackelford, 2013; Guarena et al., 2022).

The unique physico-chemical properties of bentonite clays have been shown to be beneficial for long-term containment performance of bentonite-based barriers, provided the chemistry of the containment solution is sufficiently mild (e.g. low ionic strength, neutral pH) and the bentonite exchange complex is dominated by monovalent cations (e.g. Na^+ or K^+). However, substitution of multivalent cations (e.g. Ca^{2+} or Mg^{2+}) for monovalent cations, which can occur after prolonged exposure to containment liquids that have a low monovalent-to-multivalent cation ratio, suppresses the osmotic swelling potential and can lead to an increase in hydraulic conductivity ranging from one to several orders of magnitude (Mesri and Olson, 1971; Gleason et al., 1997; Jo et al., 2001, 2004, 2005; Kolstad et al., 2004a; Katsumi et al., 2007; Bouazza and Gates, 2014). The adverse effect on hydraulic conductivity caused by the

* Corresponding author.
E-mail address: nicolo.guarena@polito.it (N. Guarena).

https://doi.org/10.1016/j.clay.2024.107318
Received 23 November 2023; Received in revised form 18 February 2024; Accepted 21 February 2024

interaction with liquids with aggressive chemistries, such as hypersaline solutions in brine evaporation ponds (AbdelRazek and Rowe, 2019), acidic leachates in mine tailing impoundments (Shackelford et al., 2010; Mazzieri et al., 2013; Liu et al., 2019), and alkaline leachates resulting from aluminum refining operations (Benson et al., 2010), is commonly referred to as chemical or hydraulic incompatibility. This evidence has stimulated research on the development of chemically modified bentonites, referred to herein as enhanced bentonites (EBs), that comprise NBs amended with organic compounds or polymers for increased resistance to chemical incompatibility upon exposure to aggressive liquids.

The commonly evaluated EBs considered for these applications can be subdivided into two broad categories on the basis of the type of chemical enhancement. The first category includes EBs that are obtained by polymerizing an organic monomer dissolved in a bentonite slurry or by directly mixing air-dried bentonite with a polymeric solution, leading to a variety of commercial products such as Bentonite Polymer Alloys (BPAs) (Trauger and Darlington, 2000), Bentonite Polymer Composites (BPCs) (Scalia, 2012), Dense Prehydrated GCLs (DPH-GCLs) (Flynn and Carter, 1998), and HYPER Clays (HCs) (Di Emidio, 2010). While all of these polymer-amended bentonites are blended with anionic (negatively charged) polymers, cationic (positively charged) polymers also have been considered as chemical additives. However, despite the benefits in terms of protection of the bentonite from adverse interactions via cation exchange, EBs amended with cationic polymers have been observed to be more susceptible to aggregation than untreated bentonites, such that the potential use of these EBs as chemical containment barriers has been limited (Di Emidio et al., 2017). The second category of EBs includes those that are treated with organic solvents which have large dielectric constants and dipole moments, such as Multiswellable Bentonites (MSBs) that are enhanced with propylene carbonate (Kondo, 1996; Onikata et al., 1996), glycerol carbonate (Fehervari et al., 2016a), or other cyclic organic carbonates (Gates et al., 2016).

The literature abounds with the results of experimental studies devoted to assessing the hydraulic compatibility of EBs upon exposure to single-salt aqueous solutions (Kolstad et al., 2004b; Katsumi et al., 2008; Malusis and McKeehan, 2013; Scalia et al., 2014; Di Emidio et al., 2015; Mazzieri and Di Emidio, 2015; Fehervari et al., 2016a; Scalia and Benson, 2017; Prongmanee et al., 2018; Tian et al., 2019; Chai and Prongmanee, 2020; Du et al., 2021; Fu et al., 2022; Norris et al., 2022, 2023), natural seawater (Mazzieri and Di Emidio, 2015; Mazzieri et al., 2017), and synthetic leachates (Mazzieri et al., 2013; Chen et al., 2019; Li et al., 2021, 2024; Zainab et al., 2021; Mazzieri and Bernardo, 2024). Experimental studies on EBs also have been conducted to measure the effective diffusion coefficient of ionic chemical species and the membrane or chemico-osmotic efficiency coefficient (Mazzieri et al., 2010; Bohnhoff and Shackelford, 2013, 2015; Bohnhoff et al., 2014; Di Emidio et al., 2015; Malusis and Daniyarov, 2016; Tong et al., 2021; Fu et al., 2021; Ni et al., 2022; Tong and Sample-Lord, 2022). However, elucidation of the pore-scale mechanisms responsible for the improved chemical compatibility of EBs relative to unenhanced NBs is still required in order to understand the long-term performance of chemical containment barriers comprising EBs.

On the basis of a comprehensive review on the available experimental evidence pertaining to the hydraulic, diffusive, and membrane behavior of EBs, Scalia et al. (2018) and Norris et al. (2023) grouped the mechanisms believed to underlie the increased chemical compatibility of EBs into three categories, namely (1) prevention of cation exchange, (2) enhanced osmotic swelling, and (3) intergranular pore clogging. While the protection of chemically modified bentonites from multivalent-for-monovalent cation exchange, which was hypothesized by Flynn and Carter (1998) and Trauger and Darlington (2000) among others, is not supported by the existing evidence (Scalia et al., 2014), enhanced osmotic swelling has been postulated by most researchers to occur in the case of MSBs. In fact, intercalation of the organic molecules (e.g. propylene carbonate) between the finest fabric units of bentonites has been shown to induce an increase in the basal spacing of the clay minerals (Onikata et al., 1999; Fehervari et al., 2016b; Gates et al., 2016) which, in turn, is regarded as the reason for the improved resistance of MSBs to chemical incompatibility. Although Kolstad et al. (2004b) and Di Emidio et al. (2015) postulated that DPH-GCLs and HCs similarly benefit from the enhancement of osmotic swelling, Scalia et al. (2018) argued that the poor correlation between swell index (SI) and k observed for BPCs and HCs suggests that the flow paths become narrower and more tortuous independent of swelling, which is likely due to partial clogging of the conductive pores by water soluble polymers, whereas the physical preconditioning of DPH-GCLs (i.e. prehydration and densification) may be the reason for the poor correlation between SI and k of DPH-GCLs.

The objective of this paper is to further elucidate the pore-scale phenomena that affect the macroscopically measured hydraulic, diffusive, and semipermeable properties of EBs under fully saturated conditions. This objective is achieved through an original interpretation of the results of the hydraulic conductivity and membrane laboratory tests published in the literature. Such interpretation is based on a theoretical framework for the coupled chemo-hydro-mechanical behavior of semipermeable porous media (e.g. bentonites) as a function of a limited number of intrinsic and state parameters, accounting for the bentonite fabric changes that are induced by a variation in the effective confining stress and the composition of the chemical solutions. The bentonite fabric is assumed to comprise nanometer-sized and micrometer-sized pores, which conceptually correspond to the interlayer and intragranular pore spaces considered by Scalia et al. (2018), respectively, with only the latter micrometer-sized pores being involved in the transport of solvent and solutes.

2. Bentonite fabric and physico-chemical modification of enhanced bentonites

2.1. Bentonite nano- and micro-pore structures

Bentonites are clays with a high content (e.g. > 70% by weight) of minerals that belong to the smectite group (Egloffstein, 2001). Typically, the main smectite constituent of bentonites is montmorillonite, a planar 2:1 type phyllosilicate mineral with a basic structural unit approximately 0.96 nm thick that comprises a single alumina octahedral sheet sandwiched between two silica tetrahedral sheets. Due to the isomorphic substitution of Al^{3+} for Si^{4+} in the tetrahedral sheet and Mg^{2+} or Fe^{2+} for Al^{3+} in the octahedral sheet, a surplus of negative electric charge is carried by montmorillonite, which typically ranges between 0.5 and 0.9 electron charges per unit cell, corresponding to a cation exchange capacity, CEC, in the 80 to 120 meq/100 g ($cmol_c$/kg) range (Grim, 1962; Mitchell and Soga, 2005; Lagaly, 2006; Sposito, 2008). The existence of this permanent surface charge is responsible for the ability of bentonites to retain inorganic and organic chemicals, heavy metals, and radionuclides (Glaus et al., 2007; Missana and García-Gutiérrez, 2007; Malusis et al., 2010) and exhibit semipermeable membrane behavior (Shackelford, 2013), phenomena that make bentonites desirable for use as chemical containment barriers. However, the aforementioned phenomena are known to be affected significantly by the chemical composition of the permeant (electrolyte) solution in that a variation in the concentration and valence (charge) of the dissolved ionic species can induce a spatial rearrangement of the montmorillonite unit layers (also referred to as lamellae or platelets) that, in turn, causes a change in the size and distribution of the bentonite pores and in the amount of the bentonite exchange sites that electrostatically interact with the mobile ions (Verburg and Baveye, 1994; Shackelford and Lee, 2003; Guyonnet et al., 2005; Tournassat and Appelo, 2011; Liu et al., 2019). Thus, any assessment of the containment performance of bentonite-based barriers should consider the macro-scale impact of the soil fabric modifications, which are controlled by the permeant chemistry, the sequence of exposure to the permeant solutions, and the soil

porosity.

The fabric of montmorillonite-rich clays is controlled by tactoids (also referred to as quasicrystals or particles) comprising from two to several thousands of montmorillonite lamellae that are stacked in a nearly parallel array (Aylmore and Quirk, 1971; Hueckel et al., 2002), thereby giving rise to nanometer-sized interlayer pores and micrometer-sized intertactoid pores. Because of the reduced void volume delimited by adjacent lamellae within the tactoids, anions are precluded from entering the interlayer pores, whereas cations needed to balance the negative structural charge of montmorillonite are bound tightly to the mineral surfaces including those in the interlayer pores and, hence, are characterized by an extremely low mobility, such that interlayer diffusion results to be of practical relevance only in the case of compacted bentonites with bulk dry densities, ρ_d, >1.0 Mg·m^{-3} (Bourg et al., 2003, 2006; García-Gutiérrez et al., 2004; Glaus et al., 2007). In contrast, anions are excluded only partially from the larger intertactoid pores, wherein the diffuse double layers can fully develop and the transport of solvent and solutes can occur relatively unimpeded.

In addition to the aforementioned differences in the transport of chemical species, the mechanisms that control the volume change behavior of the interlayer and intertactoid pores also differ. The basal spacing, d_{001}, between adjacent lamellae comprising tactoids and, thus, the extent of the so-called crystalline swelling is dictated by the number of discrete monolayers of water molecules that intercalate in the interlayer pore space, which generally varies between 2 and 3 monolayers (d_{001} approximately equal to 15 and 17 Å, respectively) when $\rho_d > 1.3$ Mg·m^{-3} and 4 monolayers (d_{001} approximately equal to 19 Å) when $\rho_d < 1.3$ Mg·m^{-3} (Kozaki et al., 1996; Muurinen et al., 2004, 2013; Matusewicz et al., 2013; Järvinen et al., 2016). Crystalline swelling is a process that occurs in the interlayer pore space and is controlled by the balance between an attractive potential energy, which is due to the negatively charged montmorillonite lamellae interacting via Coulombic and van der Waals forces, and a repulsive potential energy, which is ascribed to the hydration state of the interlayer cations. This energy balance is only weakly influenced by the electrolyte concentration of the equilibrium bulk solution (Laird, 1996; Segad et al., 2012a). Although crystalline swelling may play an important role under unsaturated soil conditions (Saiyouri et al., 2004), the volume change behavior of saturated bentonites is primarily governed by the osmotic phenomenon, i.e., the liquid flow that is caused by a difference in the osmotic pressure between the external bulk solution, which is in equilibrium with the porous medium at its boundaries, and the intertactoid pore solution (Barbour and Fredlund, 1989; Dormieux et al., 1995; Laird, 2006; Dominijanni et al., 2018). Since the extent of osmotic swelling, which takes place in the intertactoid pore space, is directly related to the thickness of the diffuse double layers that surround each individual tactoid, this phenomenon is sensitive to the chemistry of the equilibrium bulk solution.

The dual-porosity model for clays proposed by Manassero (2020), whereby the fabric of a clay comprising a parallel alignment of equally spaced tactoids is described by a single state parameter referred to as the average number of montmorillonite lamellae per tactoid, $N_{l,AV}$, is adopted herein as a conceptual scheme of the bentonite microstructure. Accordingly, the total specific surface area, S_{tot}, is subdivided into an effective specific surface area, S_{eff}, which is associated with the external surface of the tactoids interacting with the mobile portion of the pore solution, and an internal specific surface area, S_n, which is in contact with the immobile ions and water molecules within the interlayer pore space, as follows:

$$S_{eff} = \frac{S_{tot}}{N_{l,AV}} \tag{1a}$$

$$S_n = \frac{N_{l,AV} - 1}{N_{l,AV}} S_{tot} \tag{1b}$$

Based on this scenario of the bentonite fabric, a fraction of the montmorillonite lattice charge is balanced by a layer of hydrated cations specifically adsorbed on the mineral surface, commonly referred to as the Stern layer. Although the Stern layer generally is considered to behave as a hydrodynamically stagnant layer, as opposed to the diffuse part of the double layer (Lyklema et al., 1998; Delgado et al., 2007), the likelihood of tangential motion of the specifically adsorbed cations in response to gradients in the chemical and/or electrical potentials, a phenomenon known as surface conduction, is still debated (Shackelford and Moore, 2013; Leroy et al., 2015). Based on the experimental evidence obtained by Oscarson (1994) for highly compacted clay specimens, surface conduction might be of practical relevance only when $\rho_d > 1.6$ Mg·m^{-3}. Thus, the hydrated cations of the Stern layer can be considered as an immobile liquid phase for bentonite-based barriers of low-to-medium density, such as GCLs and bentonite-amended soil liners. The void ratio corresponding to the nonconductive nano-pores, e_n, including both the interlayer porosity and the Stern layer, then can be defined as follows:

$$e_n = b_n \rho_{sk} S_{tot} \left(\frac{N_{l,AV} - 1 + d_d}{N_{l,AV}} \right) \tag{2}$$

where b_n is the half distance between the lamellae in the tactoid (b_n = 0.45 nm), ρ_{sk} is the density of the solid phase, and d_d, which can be assumed equal to 4, is the thickness of the Stern layer divided by b_n (Manassero, 2020).

The void ratio corresponding to the conductive micro-pores, e_m, including the intertactoid porosity with the exclusion of the Stern layer, can be calculated as the difference between the total void ratio, e, and the nano-void ratio ($e_m = e - e_n$). The half distance between the tactoids, b_m, which also is defined as the half width of the conductive micro-channels that have a slit-like geometry, is related to the micro-void ratio according to the following relation:

$$b_m = \frac{e_m}{\rho_{sk} S_{eff}} \tag{3}$$

Some of the pore-scale mechanisms underlying the bentonite flocculation/dispersion phenomena can be framed qualitatively in the context of the Derjaguin-Landau-Verwey-Overbeek (DLVO) theory for colloidal particles (Derjaguin and Landau, 1941; Verwey and Overbeek, 1948). On the basis of the low values of the thickness-to-length ratio (< 0.01) for the montmorillonite lamellae, these can be assimilated to infinitely extended plates, such that the interaction between two adjacent lamellae mostly occurs at the crystal planes (i.e. face-to-face association), with the effect of the edge-to-edge and edge-to-face associations being negligible (Güven, 1992; Santamarina et al., 2002; Segad et al., 2012b). The total potential energy for two parallelly oriented lamellae, which can be expressed as the sum of the diffuse double layer (repulsive) potential and the van der Waals - London (attractive) potential, is a function of the concentration and electrochemical charge of the ions dissolved in the equilibrium bulk solution and the separation distance between the montmorillonite lamellae, which in turn is related to the micro-void ratio according to Eq. (3). A given set of boundary conditions then can be judged as either favorable or unfavorable towards bentonite flocculation, under the assumption that the formation of tactoids occurs when the montmorillonite lamellae get close enough to pass over the energy barrier, resulting in the drop of the total potential energy in the deep primary minimum (van Olphen, 1977; Overbeek, 1982; Novich and Ring, 1984; Luckham and Rossi, 1999; Lagaly, 2006).

Whenever the ionic concentration and/or electrochemical charge are increased under constant micro-void ratio conditions, the height of the energy barrier decreases as a result of the reduction in the repulsive potential energy. Under such conditions, bentonite flocculation can occur because of the greater likelihood of the tactoids approaching each other until their mutual attractive forces become dominant, according to a mechanism that is referred to as “Brownian motion coagulation” (Spielman, 1970; Higashitani et al., 1978). This flocculation mechanism,

which is induced by a change in the chemical composition of the equilibrium bulk solution, is expected to be favored by high values of the micro-void ratio, due to the weaker constraint to the random thermal (Brownian) motion of the clay particles. Nevertheless, compaction at a high bulk dry density (i.e. low micro-void ratio) also favors aggregation of the tactoids, which are forced to be sufficiently close to eventually yield to the mutual attractive forces, regardless of the magnitude of the electrostatic repulsive forces, with the chemical composition of the equilibrium bulk solution playing a subordinate role compared to compaction. Therefore, the aggregation state of bentonites can be interpreted as controlled by these two flocculation mechanisms, the former of which is driven by a chemical action and prevails at low-to-medium densities versus the latter which is driven by a mechanical action and prevails at higher densities.

Although the DLVO theory represents a suitable framework for a qualitative understanding of the aforementioned processes, the development of a mechanistic model that is able to quantify $N_{l,AV}$ as a function of the chemical and mechanical boundary conditions, even for the simplest case of a homogeneous and monomineral clay saturated with an aqueous solution of a single electrolyte, has never been attempted. Despite the lack of a physically sound model, the following phenomenological equation can be used to simulate the effect of the bentonite flocculation/dispersion phenomena, as proposed by Manassero et al. (2018) and Manassero (2020) in the form of the Fabric Boundary Surface (FBS):

$$N_{l,AV} = N_{l,AV0} + \frac{\alpha}{e_m}\left(\frac{c_s}{c_0}+1\right) + \beta e_m\left[1 - exp\left(-\frac{c_s}{c_0}\right)\right] \quad (4)$$

where c_s is the equivalent concentration of the electrolyte, which is hypothesized to be completely dissociated into the constituent ions, c_0 is the reference equivalent concentration (1 eq·L^{-1}), and $N_{l,AV0}$ (≥ 1), α (≥ 0), and β (≥ 0) are dimensionless parameters, which allow the microstructural arrangement of a given bentonite to be assessed while varying the electrolyte concentration of the equilibrium bulk solution and the total void ratio.

Calibration of the FBS parameters was first attempted by Manassero (2020), on the basis of the experimental results provided by Petrov and Rowe (1997), who conducted a series of hydraulic conductivity tests on conventional needle-punched GCL specimens hydrated with distilled water either prior to or after confinement and subsequently permeated with sodium chloride (NaCl) solutions with concentrations in the 0.01 to 2.0 M range. Interpretation of the Petrov and Rowe (1997) test results yielded a set of c_s, e_m, and $N_{l,AV}$ data that were fitted according to Eq. (4), thereby allowing the FBS parameters of the prehydrated needle-punched GCL to be obtained as $N_{l,AV0} = 1.56$, $\alpha = 8.82$, and $\beta = 10.01$.

2.2. Chemical amendments and manufacturing processes of enhanced bentonites

Any interpretation of the results of laboratory tests conducted on EBs requires knowledge of the specific properties of the chemical amendments, as well as the conditions under which natural bentonites are mixed with the amendments. Because of this requirement, four types of EBs have been selected for interpretation in this study due to the availability of information concerning the chemical amendments and the manufacturing processes, namely, MSB (containing propylene carbonate as amendment), DPH-GCL, HC, and BPC. Commercially available EBs that are collectively known as Contaminant Resistant Clays were not considered because of the proprietary nature of the materials and methods by the manufacturers.

2.2.1. Multiswellable Bentonites

MSBs are produced by directly mixing air-dried sodium bentonite with 15–45% (by weight) liquid propylene carbonate (PC), an aprotic polar organic solvent with a dielectric constant of 66.6 at 20 °C (Chernyak, 2006). Because of this relatively high dielectric constant compared to those for non-polar and polar organic solvents, PC molecules can coordinate with the interlayer cations of montmorillonite, preferably with cations of high polarizing power (e.g. Na^+ and Mg^{2+}), forming a cloud that surrounds the primary hydration shell of water (H_2O) molecules. After thorough mixing in a mortar, the mixture is dried and finally ground to meet the specified granule-size distribution.

Based on Fourier transform infrared absorption spectra, Onikata et al. (1999) confirmed this interaction mechanism, and X-ray diffraction (XRD) patterns recorded on powdered PC-montmorillonite complexes showed that an increase in the PC content correlated with an increase in the basal spacing of montmorillonite (up to 21 Å). A similar trend in d_{001} versus PC content was reported by Mazzieri et al. (2010) and Fehervari et al. (2016b), thus corroborating the hypothesized intercalation of PC within the interlayer space and the effectiveness of this intercalation in promoting crystalline swelling. Onikata et al. (1999) also performed XRD measurements on MSB specimens containing 45% PC that had been previously mixed with NaCl solutions of variable concentration in the 0.1 to 2 M range, and observed an abrupt increase in the estimated d_{001} value from 23 to 45 Å at a NaCl concentration equal to 0.75 M. Further increase in the d_{001} value (up to 68 Å) upon dilution of the equilibrium NaCl solution was ascribed to the transformation of crystalline swelling, which takes place in the interlayer porosity, into osmotic swelling as a result of the weakening of the bonding forces acting between the montmorillonite lamellae at high spacings ($>$ 40 Å).

Although the activation mechanism of osmotic swelling outlined by Onikata et al. (1999) also had been proposed in previous studies (e.g. Norrish and Quirk, 1954), this interpretation accounts for the presence of a single type of porosity, which corresponds to the interlayer pore space and, therefore, neglects the hierarchical nature of the bentonite pore structures and the sensitivity of the bentonite fabric to the chemical composition of the equilibrium bulk solution. If the bentonite specimen is equilibrated with a salt solution containing either divalent cations or high concentrations of monovalent cations, flocculation causes the fraction of the interlayer pore space relative to the total pore volume to increase, which is reflected as a sharp peak in the XRD pattern whereby d_{001} can be calculated reliably through Bragg's (1913) law (Moore and Reynolds, 1997). However, following tactoid exfoliation upon exposure to dilute solutions, broader diffraction peaks commonly are observed due to the decrease in the fraction of the interlayer pore space relative to the total pore volume. Under such conditions, the assessment of the angle of diffraction, at which the diffracted intensity is maximized, is affected by greater uncertainty, so that the basal spacing should be estimated by fitting the experimental data to a model diffraction pattern rather than through Bragg's (1913) law (Holmboe et al., 2012; Segad et al., 2012a).

Katsumi et al. (2008) reported results of SI tests performed with MSB specimens in equilibrium with salt solutions with ionic strengths as high as 1 M that did not indicate any overall significant improvement in osmotic swelling relative to NBs. Furthermore, Mazzieri et al. (2010) noticed the formation of unremolded, large flocs after settling of the air-dried powdered MSB at the base of the 100 mL graduated cylinder filled with a 5 mM calcium chloride ($CaCl_2$) solution. Finally, Fehervari et al. (2016a) concluded that addition of PC at extreme salt concentrations (i.e. 2 M and 5 M of NaCl, and 7.5 M of $CaCl_2$) can be detrimental to the swelling potential of MSB, as the measured SI values for MSB were lower than those for NB.

Thus, although mixing with PC does promote crystalline swelling, the existing experimental evidence does not support additional osmotic swelling as the enhancement mechanism of MSBs. This latter conclusion, despite being in conflict with the viewpoint originally advanced by Onikata et al. (1999), is consistent with the expected decrease in the ability of MSB to exhibit osmotic swelling, due to the lower dielectric constant of PC relative to that of pure water and, therefore, the reduced effectiveness of the pore solution in screening the negative electric charge of montmorillonite (Shang et al., 1994).

2.2.2. Dense Prehydrated GCLs

DPH-GCLs are manufactured by vigorously mixing dry sodium bentonite with an aqueous solution containing, among other chemical additives, the water-soluble polymer sodium carboxymethyl cellulose (Na-CMC), which is able to bind to the clay mineral surface and to intercalate within the interlayer pore space (Kolstad et al., 2004b; Qiu and Yu, 2008). In addition to the benefits arising from prehydration with the solution containing the polymer amendment, DPH-GCLs are subjected to extrusion under vacuum until a bentonite sheet of reduced thickness (~ 5 mm) and elevated bulk dry density (~ 1 $Mg{\cdot}m^{-3}$) is attained.

The exact mechanisms by which anionic polymers such as Na-CMC are adsorbed on the surface of montmorillonite crystals, including formation of hydrogen bonds and complexation via cation bridging, are still the subject of ongoing debate (Norris, 2021). However, evidence of intercalation of Na-CMC between the montmorillonite lamellae was obtained by Mazzieri and Di Emidio (2015) and Mazzieri and Bernardo (2024), who observed an increase in d_{001} through interpretation of the XRD patterns recorded on air-dried powdered clays extracted from both a conventional needle-punched GCL (d_{001} = 12.5 Å) and a DPH-GCL (d_{001} = 14.0 ÷ 15.4 Å).

Similar XRD tests were carried out by Qiu and Yu (2008) on a powdered sodium montmorillonite modified through addition of 200% (by weight) Na-CMC. Even though this weight ratio of Na-CMC to montmorillonite may not be representative of commercially available DPH-GCLs, which are manufactured with a polymer dosage of only 10% (by weight) as reported by Flynn and Carter (1998), Qiu and Yu (2008) noticed a broadening of the diffraction peak after blending with the anionic polymer, suggesting a more dispersed fabric and a lower number of montmorillonite lamellae per tactoid relative to the unamended clay. This conclusion is consistent with the evidence arising from the scanning electron micrographs (SEMs) by Mazzieri and Bernardo (2024), which confirms the effectiveness of the treatment procedure developed for DPH-GCLs in generating a highly oriented and densely packed structure of dispersed montmorillonite lamellae that is preserved after permeation with aggressive leachates.

2.2.3. HYPER Clays

HCs are bentonites modified through addition of from 2 to 16% (by weight) Na-CMC. However, instead of being vacuum-extruded like DPH-GCLs, the slurry of bentonite, polymer, and water is oven-dried at 105 °C. Di Emidio (2010) reported that dehydration at high temperature causes the polymer to irreversibly adsorb on the clay surface, thereby improving the long-term containment performance against aggressive permeant solutions due to the reduced tendency for elution of Na-CMC.

The effectiveness of such treatment procedure in intercalating Na-CMC within the interlayer pores was investigated by Di Emidio et al. (2015), who performed XRD tests on oven-dried HC specimens while varying the Na-CMC content. An increase in the polymer dosage only correlated with a slight increase in the basal spacing, from 12.35 Å for the untreated clay up to 12.41 Å for the clay treated with 16% Na-CMC. Also, the diffraction peak broadened after blending with the anionic polymer probably due to enhanced dispersion of the bentonite fabric in a manner similar to that for the modified montmorillonite tested by Qiu and Yu (2008).

2.2.4. Bentonite Polymer Composites

BPCs are obtained by vigorously mixing dry sodium bentonite with an aqueous solution containing the monomer acrylic acid, sodium hydroxide for pH neutralization, and sodium persulfate as a thermal initiator. Once the temperature of the bentonite-monomer slurry is raised above the decomposition temperature of the initiator, polymerization occurs leading to the formation of sodium polyacrylate (Na-PAA), a cross-linked, hydrophilic polymer hydrogel with a three-dimensional structure that is able to absorb large amounts of water (Scalia, 2012). When polymerization is complete, the slurry is oven-dried at 105 °C and finally ground to meet the specified granule-size distribution. The polymer content of the BPC tested by Scalia et al. (2014) was determined to be equal to 28.5% (by weight) following loss on ignition at 550 °C.

On the basis of the absence of any appreciable change in the basal spacing between powdered NB and BPC, Scalia et al. (2014) and Scalia and Benson (2017) concluded that the long-chain macromolecules of Na-PAA do not intercalate between the montmorillonite lamellae, and they hypothesized that the low k of BPCs against concentrated solutions of multivalent cations should be ascribed to the partial occlusion of the conductive (intertactoid) pores. This conclusion was corroborated by the pore-scale images of EB-GCL specimens containing anionic polyacrylamide (Tian et al., 2016, 2019), wherein the polymer hydrogel is shown to form a separate phase that fills the intertactoid pore volume.

3. Modelling the coupled transport of solvent and solutes through bentonites

The thermodynamics of irreversible processes represents a suitable framework to formulate the constitutive equations that govern the macroscopic-scale transport phenomena through electrically charged porous media (e.g. bentonites), which are able to restrict the migration of anionic species while permitting relatively unimpeded transport of solvent water (H_2O) molecules. Such selective restriction of anions, also referred to as anion exclusion or negative adsorption, is responsible for the semipermeable membrane behavior exhibited by bentonite clays, which gives rise to a number of peculiar phenomena such as hyperfiltration, chemico-osmotic counter advection, and restricted diffusion (Shackelford, 2013; Musso et al., 2017; Shackelford et al., 2019).

Given that the differences in the thermodynamic potentials across bentonite-based barriers cannot be considered small for most environmental lining applications (Yeung and Mitchell, 1993; Malusis et al., 2012), the continuous version of irreversible thermodynamics is adopted herein under the assumption that the clay membrane is homogeneous at the representative elementary volume scale and separates dilute solutions of a single salt, which is completely dissociated into the constituent ions. Accordingly, the linear relationship between the fluxes and the driving thermodynamic forces is imposed at the scale of a submembrane (Yaroshchuk, 1995) having infinitesimal thickness, dx, along the x direction, which corresponds to the macroscopic transport direction, yielding the following system of differential equations (Dominijanni and Manassero, 2012a; Malusis et al., 2021):

$$q = -k\left(\frac{\mathrm{d}h}{\mathrm{d}x} - \frac{\omega}{\gamma_w}\frac{d\Pi}{\mathrm{d}x}\right) \tag{5a}$$

$$J_s = (1-\omega)qc_s - nD_\omega^*\frac{\mathrm{d}c_s}{\mathrm{d}x} \tag{5b}$$

where q is the volumetric liquid flux, k is the hydraulic conductivity at zero electric current density, h is the hydraulic head, ω is the reflection coefficient (also known as membrane or chemico-osmotic efficiency coefficient), γ_w is the water unit weight (9.81 $kN{\cdot}m^{-3}$), $\Pi = (\nu_c + \nu_a)RTc_s$ is the osmotic pressure, ν_c and ν_a are the stoichiometric coefficients of the cation and the anion, respectively, R is the universal gas constant (8.314 $J{\cdot}mol^{-1}{\cdot}K^{-1}$), T is the absolute temperature, c_s is the concentration of the salt, J_s is the salt molar flux, n is the total porosity, and D_ω^* is the osmotic effective diffusion coefficient.

Introduction of the restrictive tortuosity factor, τ_r, which accounts for

the contribution of anion exclusion to the restriction of the diffusive salt flux through the porous medium, allows D^*_ω to be expressed as follows (Shackelford and Daniel, 1991; Malusis and Shackelford, 2002; Shackelford and Moore, 2013):

$$D^*_\omega = \tau_r D^*_s \tag{6}$$

where τ_r is a function of the reflection coefficient, the effective salt diffusion coefficient, D^*_s, and the macroscopic salt diffusion coefficient, D_s, which encompasses both molecular diffusion and the dispersive effects that are caused by the microscale fluctuations of the electric potential and the velocity field (Dominijanni et al., 2013):

$$\tau_r = (1-\omega)\frac{D_s}{D^*_s} \tag{7}$$

On the basis of the uniform-potential approach originally developed by Schmid (1950) and Schlögl (1955), Dominijanni and Manassero (2012b) derived a physical identification of the phenomenological coefficients ω and D_s. Such identification is obtained by coupling the Donnan equations with the macroscopic (i.e. upscaled through a volume-averaging technique) Navier-Stokes and Nernst-Planck equations, neglecting the microscale fluctuations of the state variables from their average values as follows:

$$\omega = 1 - \frac{\nu_c D_{a,0} + \nu_a D_{c,0}}{\nu_c \Gamma_a D_{a,0} + \nu_a \Gamma_c D_{c,0}} \Gamma_c \Gamma_a \tag{8a}$$

$$D_s = D^*_s = \tau_m D_{s,0} = \tau_m \frac{(\nu_c + \nu_a) D_{c,0} D_{a,0}}{\nu_c D_{a,0} + \nu_a D_{c,0}} \tag{8b}$$

where $D_{c,0}$ and $D_{a,0}$ are the free-solution or aqueous-phase diffusion coefficients of the cation and the anion, respectively, $D_{s,0}$ is the free-solution or aqueous-phase diffusion coefficient of the salt, Γ_c and Γ_a are the partition coefficients of the cation and the anion, respectively, and τ_m is the matrix tortuosity factor, which accounts for the tortuous nature of the conductive pores that are accessible to the transport of solvent and solutes.

Given that the partition coefficient of the i-th ionic species is defined as the ratio of the ionic concentration in the pore solution to that in the external bulk solution, which is hypothesized to be in thermodynamic equilibrium with the porous medium, assessment of Γ_c and Γ_a follows from the condition of macroscopic electroneutrality in the pore solution:

$$\Gamma_a^{-\frac{\nu_a}{\nu_c}} - \Gamma_a - \frac{\bar{c}'_{sk,0}}{\nu_c \nu_a c_s e} = 0 \tag{9a}$$

$$\Gamma_c = \Gamma_a^{-\frac{\nu_a}{\nu_c}} \tag{9b}$$

where $\bar{c}'_{sk,0}$ is the solid charge coefficient, which allows the effect of the bentonite surface charge density on the macroscopic constitutive parameters to be captured (Dominijanni et al., 2019).

In contrast to the phenomenological coefficients ω and D_s, whose physical identification is possible from the perspective of the uniform-potential approach without any specification of the microstructure of the porous medium, modelling the hydraulic conductivity as a function of the bentonite physico-chemical properties and state parameters requires a conceptual framework of the soil fabric to be defined. When the Navier-Stokes equation is integrated for the dual-porosity structural model proposed by Manassero (2020), comprising a bundle of narrow capillary fissures of constant width, $2b_m$ (cf. Eq. (3)), the following modified form of the Kozeny-Carman equation is obtained:

$$k = \tau_m \frac{\gamma_w}{3\mu_e} n \frac{e_m^2}{\left(\rho_{sk} S_{eff}\right)^2} \tag{10}$$

where μ_e is the electro-viscosity coefficient, which is equal to the dynamic viscosity of water, μ_w (10^{-3} Pa·s), under the assumption that the electro-osmotic effect due to the build-up of the streaming potential is negligible.

4. Evidence on the pore-scale interaction mechanisms in enhanced bentonites

4.1. Coupled membrane and diffusion testing

Malusis et al. (2001) and Kang and Shackelford (2009) developed closed-system laboratory apparatuses to measure the reflection coefficient of clays, consisting of either a rigid-wall or a flexible-wall modified permeameter, respectively, that allows electrolyte solutions with different chemical compositions to be circulated at the specimen boundaries under null volumetric liquid flux conditions through the porous medium. The difference in hydraulic head that establishes across the tested specimen under steady-state conditions is measured via a differential pressure transducer, such that a global value of the reflection coefficient, ω_g, corresponding to the integral mean value of ω for the given boundary osmotic pressures is obtained as follows (Dominijanni et al., 2018):

$$\omega_g = \frac{1}{\Delta\Pi} \int_{\Pi_b}^{\Pi_t} \omega \; d\Pi = \left(\frac{\gamma_w \Delta h}{\Delta\Pi}\right)_{q=0} \tag{11}$$

where $\Delta h = h_t - h_b$ and $\Delta\Pi = \Pi_t - \Pi_b$ are the differences in hydraulic head and osmotic pressure across the specimen, respectively, and the t and b subscripts denote the top and bottom specimen boundaries, respectively.

Substitution of Eq. (8a) into Eq. (11) yields the following physical identification of ω_g:

$$\omega_g = 1 - \frac{c_{s,t}\left(\nu_c \Gamma_{c,t} + \nu_a \Gamma_{a,t}\right) - c_{s,b}\left(\nu_c \Gamma_{c,b} + \nu_a \Gamma_{a,b}\right)}{\left(c_{s,t} - c_{s,b}\right)\left(\nu_c + \nu_a\right)} + \left(\frac{\bar{c}'_{sk,0}}{e}\right) \frac{D_{c,0} - D_{a,0}}{\left(c_{s,t} - c_{s,b}\right)\left(\nu_c + \nu_a\right)\left(\nu_a D_{c,0} + \nu_c D_{a,0}\right)} \ln\left(\frac{\nu_a D_{c,0} \Gamma_{c,t} + \nu_c D_{a,0} \Gamma_{a,t}}{\nu_a D_{c,0} \Gamma_{c,b} + \nu_c D_{a,0} \Gamma_{a,b}} \frac{c_{s,t}}{c_{s,b}}\right) \tag{12}$$

In addition to the measurement of the global reflection coefficient, the described laboratory apparatus allows the global value of the osmotic effective diffusion coefficient, $D^*_{\omega g}$, corresponding to the integral mean value of D^*_ω for the given boundary salt concentrations, to be determined according to the so-called steady-state or through-diffusion approach (Shackelford, 1991; Dominijanni et al., 2018):

$$D^*_{\omega g} = \frac{1}{\Delta c_s} \int_{c_{s,b}}^{c_{s,t}} D^*_\omega \; \mathrm{d}c_s = \frac{L}{n}\left[\frac{(J_s)_{ss}}{\Delta c_s}\right]_{q=0} \tag{13}$$

where L is the length of the specimen, $\Delta c_s = c_{s,t} - c_{s,b}$ is the difference in salt concentration across the specimen, and $(J_s)_{ss}$ is the steady-state value of the salt molar flux, which is calculated on the basis of the salt concentrations that are measured in the circulation outflow from the specimen boundaries.

The restrictive tortuosity factor, which is linearly related to ω_g as shown by substituting Eqs. (6) and (7) into Eq. (13), is finally calculated from the measured value of $D^*_{\omega g}$:

$$\tau_r = \left(1 - \omega_g\right) = \frac{D^*_{\omega g}}{\tau_m D_{s,0}} \tag{14}$$

Mazzieri et al. (2010), Malusis and Daniyarov (2016), Di Emidio et al. (2015), and Bohnhoff and Shackelford (2013, 2015) conducted laboratory tests for the simultaneous measurement of ω_g and $D^*_{\omega g}$ on MSB, DPH-GCL, HC, and BPC specimens, respectively, in contact with deionized water at the bottom boundary and aqueous solutions of calcium chloride ($CaCl_2$) or potassium chloride (KCl) at the top boundary.

Closed-system testing apparatuses, similar to those described by Malusis et al. (2001) and Kang and Shackelford (2009), were used for all the considered studies, with either a rigid-wall permeameter under constant volume conditions or a flexible-wall permeameter under constant effective confining stress conditions. The membrane test results have been interpreted herein according to the proposed mechanistic model, the applicability of which has been verified via the results of several studies focused on simulating coupled transport processes through NBs and GCLs (Dominijanni and Manassero, 2012b; Dominijanni et al., 2013, 2018, 2021; Musso et al., 2017; Manassero, 2020; Malusis et al., 2021; Guarena et al., 2022). The aim of the following theoretical interpretation is thus twofold, namely, to ascertain whether the application range of the proposed model can be broadened to include EBs, and to gain a deeper insight into the pore-scale interaction mechanisms that affect the macroscopic behavior of EBs.

A value of τ_m has been determined for each of the tested EB specimens by fitting the experimental values of τ_r to the theoretical relationship given by Eq. (14), as illustrated in Table 1 and Fig. 1. The free-solution diffusion coefficients of Ca^{2+}, K^+, and Cl^- were reported by Shackelford and Daniel (1991) as $D_{Ca,0} = 7.92{\cdot}10^{-10}$ $m^2{\cdot}s^{-1}$, $D_{K,0} = 19.6{\cdot}10^{-10}$ $m^2{\cdot}s^{-1}$, and $D_{Cl,0} = 20.3{\cdot}10^{-10}$ $m^2{\cdot}s^{-1}$, respectively. The value of $D^*_{\omega g}$ has been assumed to be equal to the diffusion coefficient measured for chloride ions, because steady-state diffusion for cations was not achieved in some cases due to the continual cation exchange with the cationic species originally saturating the bentonite exchange complex. Moreover, the total porosities that are reported for the single-stage membrane tests performed by Malusis and Daniyarov (2016) and the multiple-stage membrane tests performed by Bohnhoff and Shackelford (2013, 2015) using the flexible-wall cell should be regarded as average porosity values, as the tests were conducted on separate specimens in the former study and the increase in KCl concentration of the solution circulating at the upper side of the permeameter caused the specimen to consolidate during the sampling and refilling phases of the tests in the latter study.

The good agreement between the experimental data from the literature and the model predictions based on Eq. (14), as shown in Fig. 1, represents evidence that mixing with polymers or cyclic organic carbonates does not appreciably alter the physical mechanism responsible for the restriction of salt diffusion through semipermeable clay membranes, i.e., the electrostatic repulsion that partially hinders the passage of anions and, due to the requirement of null electric current density, the associated cations (Malusis et al., 2015; Dominijanni et al., 2018). In a similar way to unamended bentonites, the condition $\omega_g = 1$ is representative of an ideal membrane that is able to completely exclude salt diffusion, whereas the classical form of Fick's first law for uncharged porous media is re-established when $\omega_g = 0$.

The values of τ_m determined for EB specimens were compared with the corresponding values that were calibrated for NB and conventional GCL specimens by Musso et al. (2017), Dominijanni et al. (2018), and Manassero (2020). Irrespective of the type of testing apparatus and concentration of the salt dissolved in the permeant solution, the values of τ_m versus the total porosity closely follow a unique non-linear trend without any significant influence of the chemical amendment (Fig. 2), suggesting that the degree of interconnectivity of the conductive pores in EBs does not differ from that of unamended bentonite clays, provided the total porosity is the same. However, the τ_m values determined for the BPC tested by Bohnhoff and Shackelford (2013, 2015) are consistently lower than the overall trend for all the other bentonite specimens in the investigated porosity range. This latter observation further supports the hypothesis that the enhancement mechanism for BPCs can be ascribed to partial clogging of the conductive pores and, therefore, to more meandering channels that control solute diffusion.

According to the exponential function proposed by Olsen and Kemper (1968) to model the changes in matrix tortuosity for both saturated and unsaturated porous media, the following empirically-based relationship between τ_m and n can be established for saturated bentonite clays (Fig. 2):

$$\tau_m = \frac{\chi}{n} exp(\lambda n) \tag{15}$$

where the first set of model parameters ($\chi = 6.088{\bullet}10^{-4}$; $\lambda = 6.7049$) pertains to both NBs and EBs with the exclusion of BPCs, whereas the second set of model parameters ($\chi = 2.473{\bullet}10^{-4}$; $\lambda = 6.8859$) pertains only to BPCs, where the polymer amendment (i.e. Na-PAA) forms a three-dimensional network structure within the conductive channels, forcing the flow of water and chemicals through the remnant pores that are not occluded by the hydrogel.

Interpretation of the measured values of ω_g via calibration of $\bar{c}'_{sk,0}$ (cf. Eq. (12)) allows for the magnitude and persistence of chemico-osmosis in EBs to be assessed, as illustrated in Table 1 and Fig. 3a, b, and c for DPH-GCLs, HCs, and BPCs, respectively. Such interpretation is based on the assumption that $\bar{c}'_{sk,0}$, which is sensitive to the bentonite microstructure, is constant over the entire testing duration (Manassero, 2020), which is consistent with the negligible soil fabric changes associated with the narrow range of salt concentration that was investigated by Malusis and Daniyarov (2016), Di Emidio et al. (2015), and Bohnhoff and Shackelford (2013, 2015). The results of the single-stage membrane test conducted by Mazzieri et al. (2010) have been excluded from the theoretical interpretation, since a single value of ω_g measured at steady state ($\omega_g \simeq 0$) is not sufficient to reliably calibrate $\bar{c}'_{sk,0}$ for the tested MSB.

Table 1

Matrix tortuosity factor, τ_m, restrictive tortuosity factor, τ_r, and solid charge coefficient, $\bar{c}'_{sk,0}$, values calculated for the EB specimens subjected to coupled membrane and diffusion tests. n, total porosity; $c_{s,t}$, salt concentration of the solution circulating at the top specimen boundary; ω_g, global reflection coefficient.

	Apparatus type	Salt	n	$c_{s,t}$	ω_g	τ_m	τ_r	$\bar{c}'_{sk,0}$
			(−)	(mM)	(−)	(−)	(−)	(mM)
Mazzieri et al. (2010)	Rigid-wall cell	$CaCl_2$	0.717	5	0	0.134	1	
MSB								
Malusis and Daniyarov (2016)	Rigid-wall cell	KCl	0.608	8.7	0.73	0.051	0.384	60
DPH-GCL				160	0.15		0.906	
Di Emidio et al. (2015)	Rigid-wall cell	$CaCl_2$	0.718	1	0.65	0.137	0.241	70
HYPER Clay 2%				5	0.13		0.914	
Bohnhoff and Shackelford (2013, 2015)	Rigid-wall cell	KCl	0.92	4.7	0.84	0.154	0.325	330
BPC				54	0.21		0.715	
		KCl	0.8	4.7	0.88	0.072	0.257	140
				54	0.25		0.694	
	Flexible-wall cell	KCl	0.948	4.7	0.63	0.174	0.49	200
				54	0.07		0.835	
		KCl	0.823	4.7	0.45	0.092	0.396	70
				54	0.15		0.868	

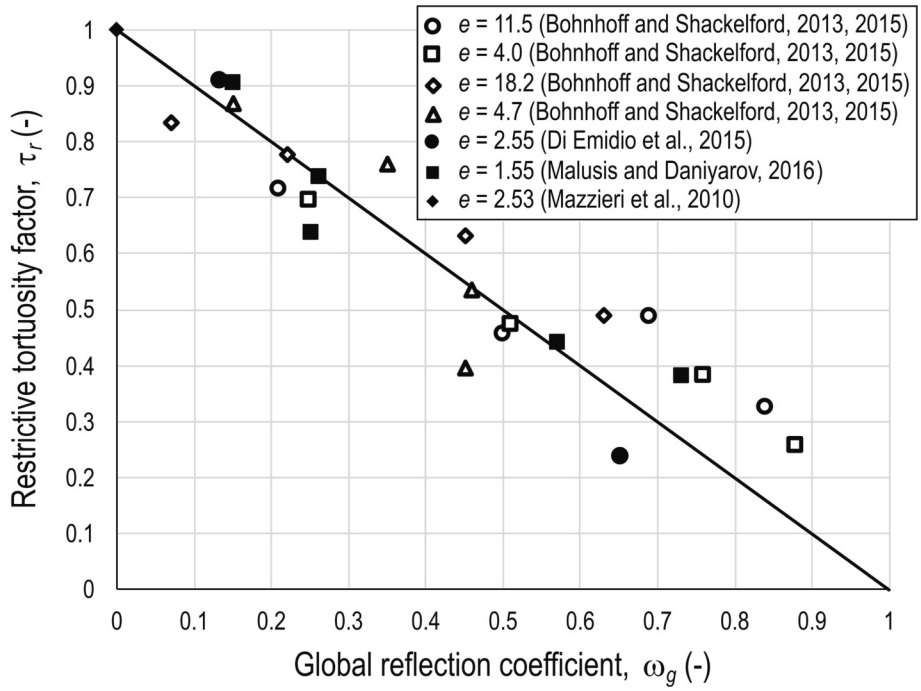

Fig. 1. Restrictive tortuosity factor values, τ_r, versus measured global reflection coefficient, ω_g, and theoretical interpretation based on Eq. (14) (continuous line). *e*, total void ratio.

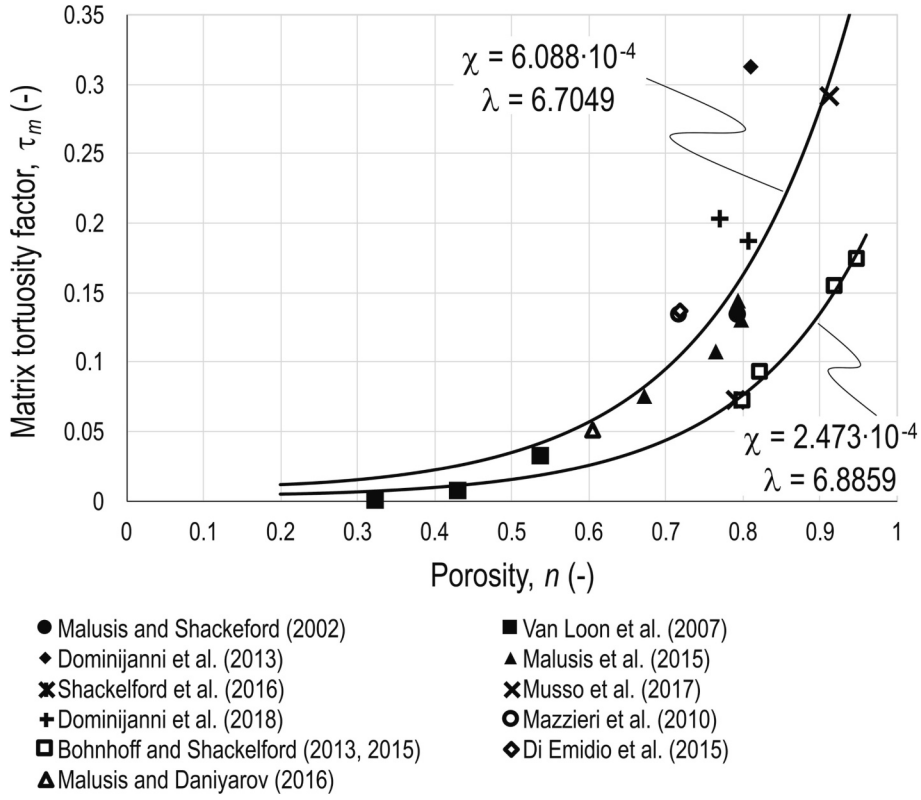

Fig. 2. Matrix tortuosity factor values, τ_m, as a function of the total porosity, *n*, for natural bentonite (closed symbols) and polymer-amended bentonite (open symbols) specimens. The continuous lines represent the interpolation curves given by Eq. (15) for NBs, MSBs, DPH-GCLs, and HCs ($\chi = 6.088 \bullet 10^{-4}$; $\lambda = 6.7049$) and for BPCs ($\chi = 2.473 \bullet 10^{-4}$; $\lambda = 6.8859$).

The adopted theoretical model quantitatively predicts the dependence of ω_g on the salt concentration of the equilibrium bulk solution for all the considered cases. Therefore, in a similar way to restricted diffusion, chemico-osmosis in polymer-amended bentonites is related to the same ionic partition effect that causes NBs to behave as selectively permeable membranes, without any appreciable influence of the

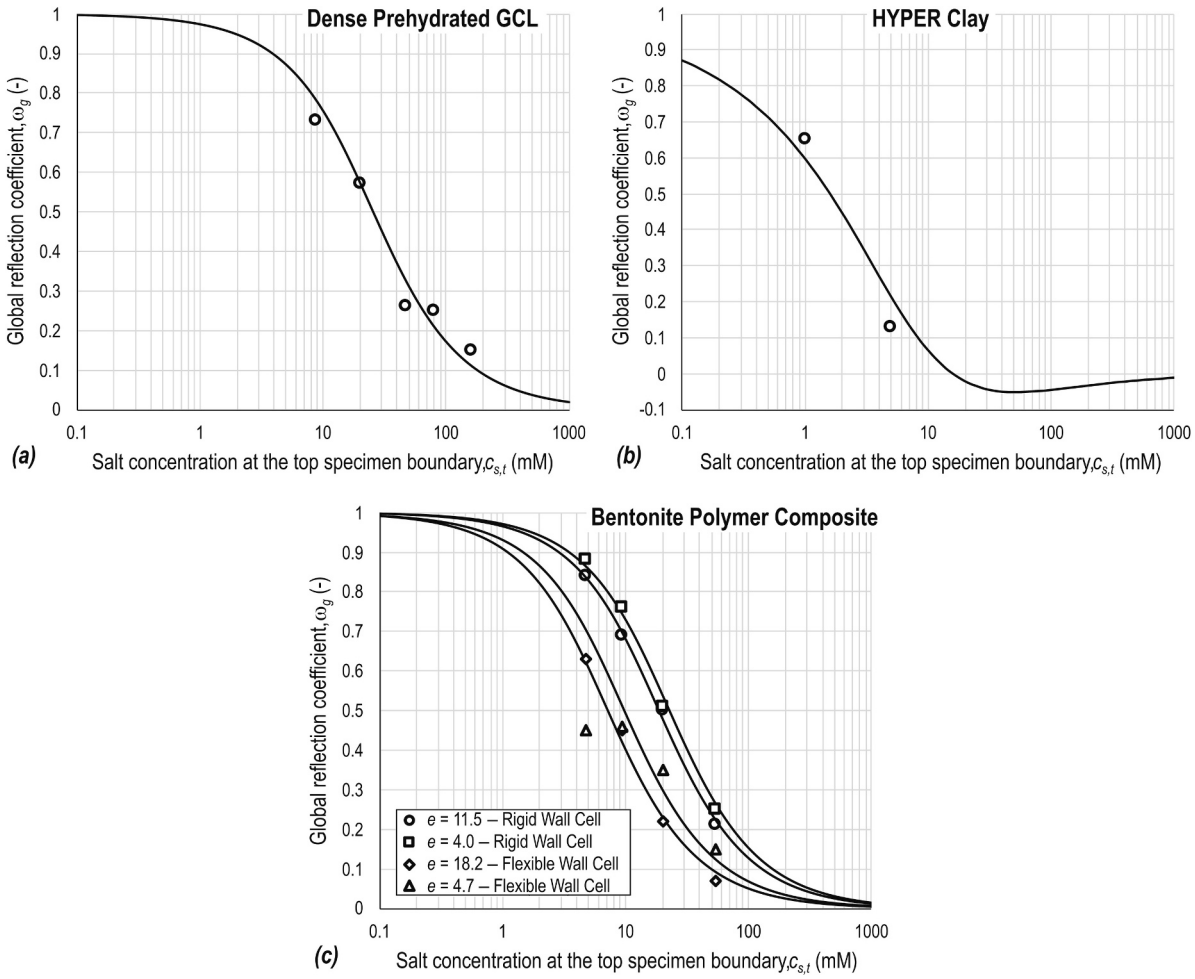

Fig. 3. Global reflection coefficient values, ω_g, as a function of the salt concentration of the solution circulating at the top specimen boundary, $c_{s,t}$, and theoretical interpretation based on Eq. (12) (continuous line) for: *(a)* the DPH-GCL tested by Malusis and Daniyarov (2016); *(b)* the HC tested by Di Emidio et al. (2015); *(c)* the BPC tested by Bohnhoff and Shackelford (2013, 2015). *e*, total void ratio.

chemical amendment either on the formation of diffuse double layers or the substitution of monovalent cations originally saturating the bentonite exchange complex with multivalent cations potentially present in the pore solution. In contrast to the polymer-amended bentonites, the complete destruction of the semipermeable membrane behavior of MSB in equilibrium with the 5 mM $CaCl_2$ solution reported by Mazzieri et al. (2010) can be explained in terms of the decrease in the thickness of the diffuse double layers, which is caused by the low dielectric constant of PC relative to that for pure water.

As discussed from a theoretical viewpoint by Dominijanni and Manassero (2012b) and verified experimentally by Dominijanni et al. (2018), the usefulness of laboratory measured reflection coefficient is not limited to characterization of coupled transport processes, since the measured reflection coefficient also provides information on the ability of the tested clay to exhibit osmotic swelling. The close relationship between the transport properties and the mechanical behavior of active clays was stressed by Dominijanni et al. (2018) through the introduction of the swell coefficient, ϖ, that quantifies how efficient a change in the salt concentration of the equilibrium bulk solution is in producing a variation in the chemico-osmotic swelling pressure, u_{sw}, which in turn is defined as the hydraulic pressure difference that develops between the pore and external bulk solutions in response to the ionic partition effect:

$$\varpi = -\frac{\mathrm{d}u_{sw}}{d\Pi} \tag{16}$$

On the basis of the same modelling assumptions underlying the physical identification of ω and D_s, ϖ is given by the following expression:

$$\varpi = 1 - \frac{\nu_c + \nu_a}{\nu_c\Gamma_a + \nu_a\Gamma_c}\Gamma_c\Gamma_a \tag{17}$$

which is identical to Eq. (8a) when cations and anions diffuse at the same rate in water (i.e. $D_{c,0} = D_{a,0}$), thus demonstrating that chemical osmosis and osmotic swelling are related to the same electrical interactions occurring between the solid skeleton and the liquid components of the pore solution.

When the external bulk solution contains a single 1:1 electrolyte (e.g. NaCl or KCl), integration of Eq. (16) allows the ratio of u_{sw} to the theoretical maximum value in equilibrium with an infinitely dilute solution, $(u_{sw})_{\Pi\to 0}$, to be expressed as follows (Dominijanni et al., 2018):

$$\frac{u_{sw}}{(u_{sw})_{\Pi\to 0}} = \eta_s\left(\sqrt{\frac{1}{\eta_s^2}+1}-1\right) \tag{18}$$

where:

$$(u_{sw})_{\Pi\to 0} = \frac{RT\bar{c}'_{sk,0}}{e} \tag{19a}$$

$$\eta_s = \frac{2ec_s}{\bar{c}'_{sk,0}} \tag{19b}$$

In terms of the relative *magnitude* of osmotic swelling in EBs and NBs,

the ratio of the maximum chemico-osmotic swelling pressure of the considered EB, $(u_{sw})^{EB}_{\Pi\to 0}$, to that of the reference NB at the same total void ratio, $(u_{sw})^{NB}_{\Pi\to 0}$, can be shown to be equal to the ratio between the corresponding values of the solid charge coefficient, $\bar{c}'^{EB}_{sk,0}$ and $\bar{c}'^{NB}_{sk,0}$ (cf. Eq. (19a)). In terms of the relative *persistence* of osmotic swelling in EBs and NBs, the ratio of the salt concentration of the considered EB, c_s^{EB}, to that of the reference NB at the same total void ratio, c_s^{NB}, that causes the same percent decrease in the chemico-osmotic swelling pressure relative to the theoretical maximum value can be obtained from the condition of equality between the corresponding dimensionless state parameters η_s. Based on this condition and the definition of η_s (cf. Eq. (19b)), the ratio of c_s^{EB} to c_s^{NB} is again equal to the ratio of $\bar{c}'^{EB}_{sk,0}$ to $\bar{c}'^{NB}_{sk,0}$.

The reference NB, selected herein for assessing whether the physico-chemical modifications of EBs correlate with an improved ability to exhibit osmotic swelling, is the powdered sodium bentonite tested by Dominijanni et al. (2018) that is used for the industrial production of a conventional needle-punched GCL. Interpretation of the laboratory tests, which were conducted by Dominijanni et al. (2018) through a modified strain-controlled oedometer cell that allows ω and ϖ to be simultaneously measured on the same clay specimen, resulted in a solid charge coefficient, $\bar{c}'^{NB}_{sk,0}$, equal to 110 mM. According to Dominijanni et al. (2021), the variations in $\bar{c}'^{NB}_{sk,0}$ are expected to be limited for the powdered sodium bentonites that are used within chemical containment barriers, thus supporting the generality of the conclusions drawn for $\bar{c}'^{NB}_{sk,0} = 110$ mM. The values of the solid charge coefficient, $\bar{c}'^{EB}_{sk,0}$, calibrated for the DPH-GCL tested by Malusis and Daniyarov (2016), the HC tested by Di Emidio et al. (2015), and the BPC tested by Bohnhoff and Shackelford (2013, 2015), are reported in Table 1.

In the case of polymer-amended bentonites, the evidence that emerges from Fig. 4, wherein the ratios $(u_{sw})^{EB}_{\Pi\to 0}/(u_{sw})^{NB}_{\Pi\to 0}$ and c_s^{EB}/c_s^{NB} are shown versus the total void ratio, does not support enhanced magnitude and persistence of osmotic swelling as a mechanism that contributes to overcoming the limitations of NBs and conventional GCLs when liquids with aggressive chemistries are to be contained. Despite not being quantitatively assessed, the detrimental effect of the 5 mM $CaCl_2$ solution on the semipermeable membrane behavior of the MSB tested by Mazzieri et al. (2010) further suggests that liquid PC acts as inhibitor of osmotic swelling, due to a reduced ability to screen the negative electric charge of montmorillonite compared to pure water.

4.2. Hydraulic conductivity testing

Among various indirect methods to evaluate the pore structure of fully-saturated bentonites, interpretation of hydraulic conductivity test results has been recognized as suitable to investigate flocculation/dispersion phenomena over a wide range of soil porosities and salt concentrations of the permeant solution, since the hydraulic conductivity can vary over several orders of magnitude as a result of a variation in the bentonite fabric (Guarena et al., 2020; Manassero, 2020). Such interpretation relies on the use of Eq. (10), which provides a value of $N_{l,AV}$ for each measured value of k once a limited number of intrinsic and state parameters (S_{tot}, ρ_{sk}, and e) of the tested bentonite are known and τ_m is assessed via Eq. (15).

The long-term hydraulic conductivity tests with single-salt permeant solutions performed by Katsumi et al. (2008) for MSB and DPH-GCL specimens, Kolstad et al. (2004b) and Malusis and Daniyarov (2016) for DPH-GCL specimens, Di Emidio et al. (2015) for an HC specimen, and Scalia et al. (2014) for BPC specimens, have all been interpreted herein to gain insight into the microstructural arrangement of these EBs, and the resulting values of $N_{l,AV}$ are summarized in Table 2. Note that the DPH-GCL specimens tested by Malusis and Daniyarov (2016) and the HC specimen tested by Di Emidio et al. (2015) were subjected to simultaneous measurements of the semipermeable and diffusion properties and, hence, the corresponding values of τ_m that were used in Eq. (10) have been assumed to be equal to the values calibrated from the interpretation of the measured ω_g and $D^*_{\omega g}$ (Table 1).

In addition to the aforementioned studies, the hydraulic conductivity values that were measured by Norris et al. (2022) on specimens of an EB-GCL, modified through wet mixing with Na-CMC of low viscosity (CMCLV) and high viscosity (CMCHV), have been considered, in an attempt to cover the current paucity of data on HCs. Considering the analogies in the treatment procedures of the HC specimen tested by Di

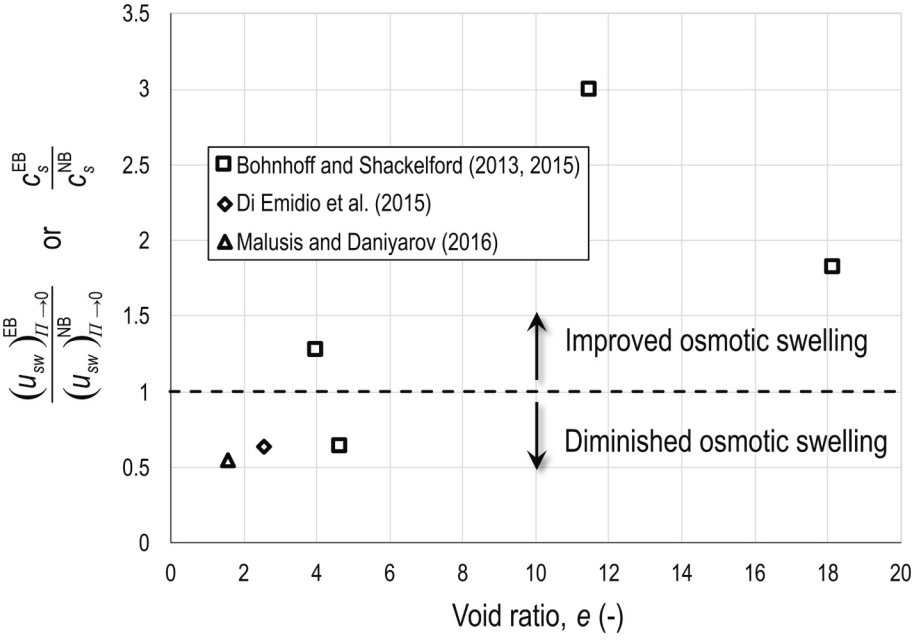

Fig. 4. Relative magnitude, $(u_{sw})^{EB}_{\Pi\to 0}/(u_{sw})^{NB}_{\Pi\to 0}$, and persistence, c_s^{EB}/c_s^{NB}, of osmotic swelling in EBs and NBs, as a function of the total void ratio, e. $(u_{sw})^{EB}_{\Pi\to 0}$ and $(u_{sw})^{NB}_{\Pi\to 0}$, maximum chemico-osmotic swelling pressures of the considered EB and the reference NB, respectively. c_s^{EB} and c_s^{NB}, salt concentrations of the considered EB and the reference NB, respectively, which cause the same percent decrease in the chemico-osmotic swelling pressure relative to the maximum value.

Table 2
Range of intrinsic, state, and fabric parameters of the EB specimens subjected to hydraulic conductivity tests. ρ_{sk}, solid phase density; e, total void ratio; c_s, equivalent salt concentration of the permeant solution; k, hydraulic conductivity; $N_{l,AV}$, average number of montmorillonite lamellae per tactoid.

	Specimen type	Salt	CEC [(a)]	ρ_{sk}	e	c_s	k	$N_{l,AV}$
			(meq/100 g)	($Mg{\cdot}m^{-3}$)	(−)	($meq{\cdot}L^{-1}$)	($m{\cdot}s^{-1}$)	(−)
Katsumi et al. (2008)	MSB	NaCl	82.0	2.478	0.905	0	$7.0{\cdot}10^{-12}$	8.87
		$CaCl_2$			2.407	2000	$2.6{\cdot}10^{-9}$	236.7
	DPH-GCL	$CaCl_2$	104.0	2.73	2.249	500	$1.2{\cdot}10^{-12}$	5.11
					2.782	2000	$3.6{\cdot}10^{-12}$	9.49
Kolstad et al. (2004b)	DPH-GCL	NaCl	84.1 [(b)]	2.5	1.2	0	$3.7{\cdot}10^{-12}$	36.92
		$CaCl_2$				2000	$4.2{\cdot}10^{-12}$	38.94
Malusis and Daniyarov (2016)	DPH-GCL	KCl	52	2.69	1.128	0	$7.0{\cdot}10^{-13}$	4.26
					1.778	160	$2.0{\cdot}10^{-12}$	11.67
Di Emidio et al. (2015)	HYPER Clay 2%	$CaCl_2$	47.29	2.53	2.546	0	$5.3{\cdot}10^{-12}$	2.62
						10	$6.5{\cdot}10^{-12}$	2.83
Norris et al. (2022)	CMCLV EB-GCL	NaCl	78.0	2.76	2.429	334	$6.7{\cdot}10^{-11}$	15.05
		$CaCl_2$			2.843	500	$4.1{\cdot}10^{-10}$	49.35
	CMCHV EB-GCL	NaCl	78.0	2.76	2.926	334	$2.3{\cdot}10^{-11}$	7.19
		$CaCl_2$			3.257	500	$3.8{\cdot}10^{-10}$	32.25
Scalia et al. (2014)	BPC	$CaCl_2$	85.5	2.71	1.6	0	$1.8{\cdot}10^{-11}$	1.15
					13.5	400	$8.1{\cdot}10^{-11}$	90.12

(a) As discussed by Shang et al. (1994), the cation exchange capacity, CEC, can be related to the total specific surface area, S_{tot}, according to the CEC $= \sigma S_{tot}/F$ relation, where σ is the surface charge density of montmorillonite ($0.114 C{\cdot}m^{-2}$) and F is Faraday's constant ($9.6485{\bullet}10^{-4} C{\cdot}mol^{-1}$).
(b) The CEC value of the DPH-GCL specimens tested by Kolstad et al. (2004b) has been estimated from the smectite content (89%), which was determined by means of XRD.

Emidio et al. (2015) and the CMC amended EB-GCL specimens tested by Norris et al. (2022), both of these EBs are expected to show a similar type of behavior, even though the aforementioned treatment procedures were not exactly identical, with differences in terms of the polymer dosage (2% vs 5% by dry weight), the mixing time of the slurry of bentonite, polymer, and water (30 min vs 10 min), and the grain-size distribution after oven-drying, grinding, and sieving.

In Fig. 5, the $N_{l,AV}$ values resulting from the interpretation of the k measurements on EBs are shown versus the micro-void ratio, and also compared with the corresponding isoconcentration curves of the FBS for prehydrated, conventional GCLs. The purpose of this comparison is to evaluate the differences that exist between the aggregation states of NBs hydrated with distilled water, the behavior of which is assumed to be comparable with that of the GCL tested by Petrov and Rowe (1997), versus the considered EBs, in equilibrium with both the dilute and concentrated electrolyte solutions used to simulate aggressive leachates. Thus, an assessment of the impact of the chemical amendment on the sensitivity of the bentonite fabric to the salt concentration of the permeant solution and to the bentonite porosity is possible.

As shown in Fig. 5a and aside from the data for permeation with deionized water, all the calculated values of $N_{l,AV}$ for the non-prehydrated MSB specimens tested by Katsumi et al. (2008) are consistently greater than the model predictions for prehydrated NBs. The observed increase in $N_{l,AV}$ under the same chemical composition of the permeant solution can be ascribed, in part, to the absence of exposure to deionized water prior to permeation with the testing solutions (Shackelford et al., 2000). However, the decrease in the measured k for the MSB specimens subjected to intermediate NaCl concentrations ($200 \leq c_s \leq 1000$ $meq{\cdot}L^{-1}$), relative to the results of comparative permeability tests carried out by Katsumi et al. (2008) on unamended (non-prehydrated) bentonite specimens, should be interpreted in view of the modification of the bentonite swelling behavior, which is due to mixing with liquid PC. Although the effectiveness of PC in promoting crystalline swelling has been corroborated by an extensive experimental evidence, the results of the SI tests conducted to date have not indicated any significant difference between MSBs and NBs in terms of exhibiting osmotic swell (see Subsection 2.2.1). Also, in some cases, evidence of a greater compressibility of the solid skeleton, which must result at the expense of a reduction in the intertactoid porosity, was obtained for MSBs. Such evidence is further confirmed by the greater volumetric compressive strain that was experienced by the MSB specimens tested by Katsumi et al. (2008), which were consolidated up to an average total void ratio of 0.963 for the NaCl concentrations in the 200 to 1000 $meq{\cdot}L^{-1}$ range. Upon completion of consolidation, the MSB specimens were characterized by an appreciably lower total void ratio than the values ($1.971 \leq e \leq 3.046$) associated with the unamended bentonite specimens subjected to comparative permeability tests, under the same effective confining stress and the same chemical composition of the permeant solution. According to Eq. (10), the greater compressibility of the solid skeleton, which is reflected by the low values of the micro-void ratio shown in Fig. 5a, can be regarded as the reason for the observed decrease in k.

Unlike MSBs, the ability of DPH-GCLs to maintain a dispersed bentonite fabric and, hence, an extremely low hydraulic conductivity ($k \sim 10^{-12}$ $m{\cdot}s^{-1}$) upon permeation with concentrated $CaCl_2$ solutions is reflected by the values of $N_{l,AV}$ that lie close to the isoconcentration curve for deionized water (Fig. 5b). This behavior can be attributed to the aforementioned treatment procedure developed for DPH-GCLs, which involves prehydration of the dry sodium bentonite with the polymeric solution, followed by preconsolidation (densification) through vacuum extrusion. After intercalation between the montmorillonite lamellae during manufacturing, the adsorbed anionic polymer prevents the mineral surfaces from coming together and yielding to their mutual attractive forces, according to a mechanism that is referred to as "steric stabilization" (Overbeek, 1982; Luckham and Rossi, 1999), and thus inhibits the flocculation mechanism related to the increase in the ionic strength of the pore solution. The observed agreement between the calculated values of $N_{l,AV}$ and the isoconcentration curve based on deionized water at the lowest e_m also indicates that the same treatment procedure is not effective in hindering aggregation when DPH-GCLs are consolidated under a high effective confining stress, since the flocculation mechanism related to compaction is not affected by the polymer intercalation between the montmorillonite lamellae.

Low k values also were evident for the HC specimen, which are consistent with the low calculated values of $N_{l,AV}$ (Fig. 5c). However, the salt solutions used by Di Emidio et al. (2015) for HC were not sufficiently concentrated to allow for an assessment of the influence of Na-CMC on the aggregation state of the modified bentonite upon exposure to harsh chemical environments. Although the preparation of HC involves a similar polymeric solution to that used for DPH-GCLs, the slurry of bentonite, polymer, and water is oven-dried at 105 °C instead of being vacuum-extruded and, as such, the potential contribution of densification to the long-term barrier performance is excluded. The results of the

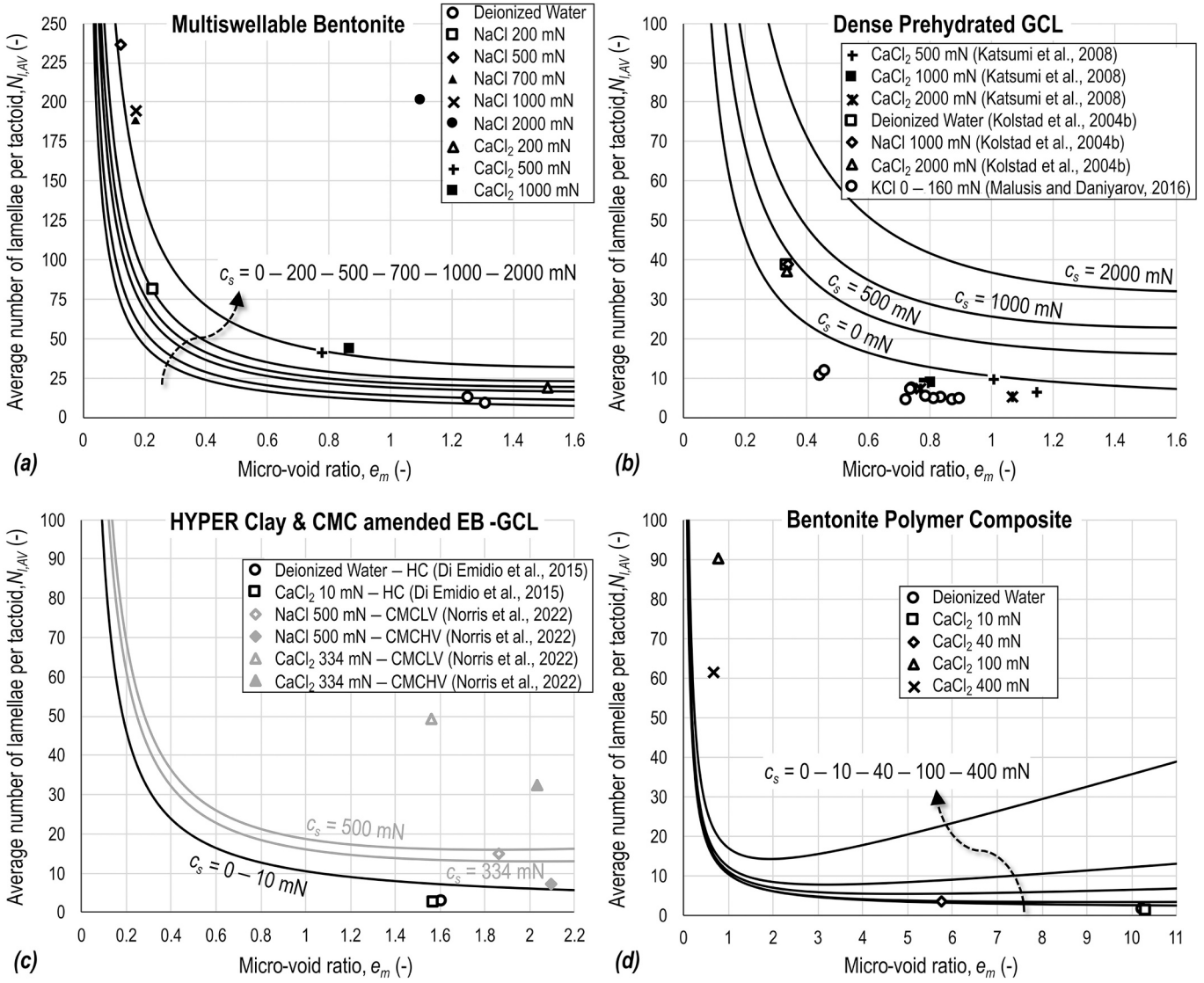

Fig. 5. Comparison between the isoconcentration curves of the FBS (continuous lines), calibrated on the hydraulic conductivity test results of Petrov and Rowe (1997), and the values of the average number of montmorillonite lamellae per tactoid, $N_{l,AV}$, obtained from interpretation of the measured hydraulic conductivity of: *(a)* the MSB tested by Katsumi et al. (2008); *(b)* the DPH-GCL tested by Katsumi et al. (2008), Kolstad et al. (2004b), and Malusis and Daniyarov (2016); *(c)* the HC tested by Di Emidio et al. (2015) and the CMC amended EB-GCL tested by Norris et al. (2022); *(d)* the BPC tested by Scalia et al. (2014). c_s, equivalent salt concentration of the permeant solution.

permeability tests performed by Norris et al. (2022) on non-prehydrated CMC amended EB-GCL specimens have been interpreted with the aim of addressing this latter issue, and the corresponding $N_{l,AV}$ values are reported in gray in Fig. 5c. These results suggest that the polymer viscosity plays a relevant role in determining the bentonite fabric, with the high viscosity Na-CMC being more effective in favoring a dispersed and highly porous microstructure than the low viscosity Na-CMC. Furthermore, the possibility of maintaining a dispersed fabric upon permeation with high ionic strength aqueous solutions depends to a great extent on the electrochemical charge of the cationic species that result from the salt dissociation. In the case of a prevalence of monovalent cations (e.g. Na^+), blending with Na-CMC may be associated with values of $N_{l,AV}$ that are lower than or comparable with the model predictions for prehydrated NBs, whereas the presence of divalent cations is detrimental to the ability of Na-CMC to prevent the bentonite from flocculating at high salt concentrations. On the basis of such evidence, the contribution of densification to the long-term barrier performance may be a primary consideration, particularly when low viscosity Na-CMC is used and multivalent cations are contained in the permeant solution. However, further study is needed on HC, prepared according to the treatment procedure described by Di Emidio et al. (2015), to verify this conclusion.

The relatively high values of $N_{l,AV}$ observed for the non-prehydrated BPC specimens tested at the highest $CaCl_2$ concentrations (Fig. 5d) can be attributed, as for the MSB specimens, to direct permeation with the chemical solutions, i.e., without prehydration. Given that Na-PAA does not prevent aggregation of the bentonite microstructure upon contact with concentrated electrolyte solutions, the reduction in hydraulic conductivity noted by Scalia et al. (2014) relative to the results of comparative hydraulic conductivity tests conducted with unamended (non-prehydrated) bentonite specimens can be correlated with the low values of τ_m that result from Eq. (15) and the low values of e_m observed in Fig. 5d. However, unlike MSBs, the decrease in the pore space accessible to the solvent and solute transport with increasing $CaCl_2$ concentration is caused by the polymer hydrogel that partially occludes the bentonite pores, with this latter mechanism being corroborated in a number of published studies (see Subsection 2.2.4). For the sake of comparison, no evidence of polymer strands or web binding to the tactoids is apparent in the SEMs reported by Mazzieri and Bernardo (2024), thus reinforcing

the hypothesis that the mechanism governing the hydraulic and chemical transport behavior of BPCs (i.e. partial clogging of the conductive pores) is substantially different from that of DPH-GCLs (i.e. enhanced dispersion of the bentonite fabric, due to intercalation of Na-CMC between the montmorillonite lamellae and densification through vacuum extrusion).

5. Conclusions

The available literature pertaining to the laboratory assessment of the semipermeable, diffusive, and hydraulic properties of enhanced bentonites (EBs) was interpreted via a theoretical model that allows the measured macroscopic transport parameters (i.e. the reflection coefficient, ω, the osmotic effective diffusion coefficient, D_{ω}^{*}, and the hydraulic conductivity, k) to be related to a limited number of intrinsic and state parameters, which include the average number of montmorillonite lamellae per tactoid, $N_{l,AV}$, that accounts for the bentonite fabric and the matrix tortuosity factor, τ_m, that accounts for the degree of interconnectivity of the conductive pores. The study focused on four EBs, namely, Multiswellable Bentonites (MSBs), Dense Prehydrated GCLs (DPH-GCLs), HYPER Clays (HCs), and Bentonite Polymer Composites (BPCs), with the objective of further elucidating the interaction mechanisms between the solid bentonite phase and the chemical additives.

On the basis of the available membrane test results, enhanced osmotic swelling, which was suggested by Scalia et al. (2018) as one of the three possible mechanisms believed to influence the behavior of EBs, has herein been discounted as a factor that contributes to improving the sealing ability of all the considered EBs. In the case of MSBs, this conclusion has been further corroborated by a greater compressibility relative to unamended bentonites subjected to comparative hydraulic conductivity tests, thus suggesting that propylene carbonate acts as inhibitor of osmotic swelling. The greater volumetric compressive strain experienced by MSBs must occur at the expense of a reduction in the intertactoid porosity, which in turn is responsible for the observed decrease in measured k.

Intergranular pore clogging has been confirmed as the primary mechanism that controls the k of BPCs upon permeation with aqueous solutions with high ionic strength. However, as a difference from MSBs, partial occlusion of the pore space by the polymer hydrogel not only leads to a reduction in the conductive porosity, but also causes the remnant conductive pores to be more tortuous and meandering in the case of BPCs, as demonstrated by low values of τ_m.

DPH-GCLs are characterized by a low k upon exposure to concentrated electrolyte solutions as a result of an enhanced dispersion of the bentonite fabric, which is an additional mechanism relative to those described by Scalia et al. (2018), and is attributed to the combined effect of prehydration with the polymeric solution and preconsolidation through vacuum extrusion. However, this same ability to maintain a dispersed fabric was not observed for MSBs and BPCs, which undergo more extensive flocculation (i.e. higher $N_{l,AV}$) than prehydrated natural bentonites when the specimens are directly permeated with the concentrated electrolyte solutions. Although a similar polymeric solution to that of DPH-GCLs is used in the preparation of HCs, additional study is recommended to verify whether HC can benefit from the aforementioned mechanism, i.e., preservation of a dispersed bentonite fabric, even in the absence of the preconsolidation effect.

Declaration of funding sources

This research did not receive any specific grant from funding agencies in the public, commercial, or not-for-profit sectors.

CRediT authorship contribution statement

Nicolò Guarena: Writing – review & editing, Writing – original draft, Visualization, Methodology, Investigation, Formal analysis, Conceptualization. **Andrea Dominijanni:** Supervision, Methodology. **Mario Manassero:** Writing – review & editing, Supervision, Conceptualization.

Declaration of competing interest

The authors declare that they have no known competing financial interests or personal relationships that could have appeared to influence the work reported in this paper.

Data availability

Data will be made available on request.

Acknowledgments

The authors are grateful to Prof. Charles Shackelford (Colorado State University, Fort Collins, Colorado, USA) for the careful and insightful review of this article.

References

AbdelRazek, A.Y., Rowe, R.K., 2019. Performance of GCLs in high salinity impoundment applications. Geosynth. Int. 26 (6), 611–628. https://doi.org/10.1680/jgein.19.00043.

Aylmore, L.A.G., Quirk, J.P., 1971. Domains and quasi-crystalline regions in clay systems. Soil Sci. Soc. Am. J. 35 (4), 652–654. https://doi.org/10.2136/sssaj1971.03615995003500040046x.

Barbour, S.L., Fredlund, D.G., 1989. Mechanisms of osmotic flow and volume change in clay soils. Can. Geotech. J. 26 (4), 551–562. https://doi.org/10.1139/t89-068.

Benson, C.H., Ören, A.H., Gates, W.P., 2010. Hydraulic conductivity of two geosynthetic clay liners permeated with a hyperalkaline solution. Geotext. Geomembr. 28 (2), 206–218. https://doi.org/10.1016/j.geotexmem.2009.10.002.

Bohnhoff, G.L., Shackelford, C.D., 2013. Improving membrane performance via bentonite polymer nanocomposite. Appl. Clay Sci. 86, 83–98. https://doi.org/10.1016/j.clay.2013.09.017.

Bohnhoff, G.L., Shackelford, C.D., 2015. Salt diffusion through a bentonite-polymer composite. Clay Clay Miner. 63 (3), 145–162. https://doi.org/10.1346/CCMN.2015.0630301.

Bohnhoff, G.L., Shackelford, C.D., Sample-Lord, K.M., 2014. Calcium-resistant membrane behavior of polymerized bentonite. J. Geotech. Geoenviron. Eng. 140 (3), 04013029. https://doi.org/10.1061/(ASCE)GT.1943-5606.0001042.

Bouazza, A., 2002. Geosynthetic clay liners. Geotext. Geomembr. 20 (1), 3–17. https://doi.org/10.1016/S0266-1144(01)00025-5.

Bouazza, A., Gates, W.P., 2014. Overview of performance compatibility issues of GCLs with respect to leachates of extreme chemistry. Geosynth. Int. 21 (2), 151–167. https://doi.org/10.1680/gein.14.00006.

Bourg, I.C., Bourg, A.C.M., Sposito, G., 2003. Modeling diffusion and adsorption in compacted bentonite: a critical review. J. Contam. Hydrol. 61 (1–4), 293–302. https://doi.org/10.1016/S0169-7722(02)00128-6.

Bourg, I.C., Sposito, G., Bourg, A.C.M., 2006. Tracer diffusion in compacted, water-saturated bentonite. Clay Clay Miner. 54 (3), 363–374. https://doi.org/10.1346/CCMN.2006.0540307.

Bragg, W.H., 1913. The reflection of X-rays by crystals. Nature 91 (2280), 477. https://doi.org/10.1038/091477b0.

Brandl, H., 1994. Vertical barriers for municipal and hazardous waste containment. In: Balasubramaniam, A.S., Hong, S.W., Bergado, D.T., Phien-Wej, N., Nutalaya, P. (Eds.), Proceedings of the Symposium on Developments in Geotechnical Engineering. CRC Press/Balkema, pp. 301–334.

Chai, J.C., Prongmanee, N., 2020. Barrier properties of a geosynthetic clay liner using polymerized sodium bentonite. Geotext. Geomembr. 48 (3), 392–399. https://doi.org/10.1016/j.geotexmem.2019.12.010.

Chen, J., Salihoglu, H., Benson, C.H., Likos, W.J., Edil, T.B., 2019. Hydraulic conductivity of bentonite-polymer composite geosynthetic clay liners permeated with coal combustion product leachates. J. Geotech. Geoenviron. Eng. 145 (9), 04019038. https://doi.org/10.1061/(ASCE)GT.1943-5606.0002105.

Chernyak, Y., 2006. Dielectric constant, dipole moment, and solubility parameters of some cyclic acid esters. J. Chem. Eng. Data 51 (2), 416–418. https://doi.org/10.1021/je050341y.

Delgado, A.V., González-Caballero, F., Hunter, R.J., Koopal, L.K., Lyklema, J., 2007. Measurement and interpretation of electrokinetic phenomena. J. Colloid Interface Sci. 309 (2), 194–224. https://doi.org/10.1016/j.jcis.2006.12.075.

Derjaguin, B.V., Landau, L., 1941. Theory of the stability of strongly charged lyophobic sols and the adhesion of strongly charged particles in solutions of electrolytes. Acta Physicochim. URSS 14, 633–662.

Di Emidio, G., 2010. Hydraulic and chemico-osmotic performance of polymer treated clays [Doctoral dissertation, Ghent University]. Ghent University Theses and Dissertations Archive. https://biblio.ugent.be/publication/1009935.

Di Emidio, G., Mazzieri, F., Verastegui-Flores, R.D., Van Impe, W., Bezuijen, A., 2015. Polymer-treated bentonite clay for chemical-resistant geosynthetic clay liners. Geosynth. Int. 22 (1), 125–137. https://doi.org/10.1680/gein.14.00036.

Di Emidio, G., Verastegui-Flores, R.D., Mazzieri, F., Dominijanni, A., 2017. Modified clays for barriers: a review. Innov. Infrastruct. Solut. 2 (1), 47. https://doi.org/10.1007/s41062-017-0073-8.

Dominijanni, A., Manassero, M., 2012a. Modelling the swelling and osmotic properties of clay soils. Part I: the phenomenological approach. Int. J. Eng. Sci. 51, 32–50. https://doi.org/10.1016/j.ijengsci.2011.11.003.

Dominijanni, A., Manassero, M., 2012b. Modelling the swelling and osmotic properties of clay soils. Part II: the physical approach. Int. J. Eng. Sci. 51, 51–73. https://doi.org/10.1016/j.ijengsci.2011.11.001.

Dominijanni, A., Manassero, M., Puma, S., 2013. Coupled chemical-hydraulic-mechanical behaviour of bentonites. Géotechnique 63 (3), 191–205. https://doi.org/10.1680/geot.SIP13.P.010.

Dominijanni, A., Guarena, N., Manassero, M., 2018. Laboratory assessment of semipermeable properties of a natural sodium bentonite. Can. Geotech. J. 55 (11), 1611–1631. https://doi.org/10.1139/cgj-2017-0599.

Dominijanni, A., Fratalocchi, E., Guarena, N., Manassero, M., Mazzieri, F., 2019. Critical issues in the determination of the bentonite cation exchange capacity. Géotech. Lett. 9 (3), 205–210. https://doi.org/10.1680/jgele.18.00229.

Dominijanni, A., Guarena, N., Manassero, M., 2021. The role of chemico-osmosis in the performance assessment of bentonite-based contaminant barriers. J. Phys. Conf. Ser. 1928, 012008 https://doi.org/10.1088/1742-6596/1928/1/012008.

Dormieux, L., Barboux, P., Coussy, O., Dangla, P., 1995. A macroscopic model of the swelling phenomenon of a saturated clay. Eur. J. Mech. A/Solids 14 (6), 981–1004.

Du, Y.J., Shen, S.Q., Tian, K., Yang, Y.L., 2021. Effect of polymer amendment on hydraulic conductivity of bentonite in calcium chloride solutions. J. Mater. Civ. Eng. 33 (2), 04020452. https://doi.org/10.1061/(ASCE)MT.1943-5533.0003518.

Egloffstein, T.A., 2001. Natural bentonites - Influence of the ion exchange and partial desiccation on permeability and self-healing capacity of bentonites used in GCLs. Geotext. Geomembr. 19 (7), 427–444. https://doi.org/10.1016/S0266-1144(01)00017-6.

Fehervari, A., Gates, W.P., Patti, A.F., Turney, T.W., Bouazza, A., Rowe, R.K., 2016a. Potential hydraulic barrier performance of cyclic organic carbonate modified bentonite complexes against hyper-salinity. Geotext. Geomembr. 44 (5), 748–760. https://doi.org/10.1016/j.geotexmem.2016.06.002.

Fehervari, A., Gates, W.P., Turney, T.W., Patti, A.F., Bouazza, A., 2016b. Cyclic organic carbonate modification of sodium bentonite for enhanced containment of hyper saline leachates. Appl. Clay Sci. 134, 2–12. https://doi.org/10.1016/j.clay.2016.09.007.

Flynn, B., Carter, G. (1998). *Waterproofing material and method of fabrication thereof* (U.S. Patent No. 6,537,676 B1). U.S. Patent and Trademark Office.

Fu, X.L., Zhang, R., Reddy, K.R., Li, Y.C., Yang, Y.L., Du, Y.J., 2021. Membrane behavior and diffusion properties of sand/SHMP-amended bentonite vertical cutoff wall backfill exposed to lead contamination. Eng. Geol. 284, 106037 https://doi.org/10.1016/j.enggeo.2021.106037.

Fu, X.L., Shen, S.Q., Reddy, K.R., Yang, Y.L., Du, Y.J., 2022. Hydraulic conductivity of sand/biopolymer-amended bentonite backfills in vertical cutoff walls permeated with lead solutions. J. Geotech. Geoenviron. Eng. 148 (2), 04021186. https://doi.org/10.1061/(ASCE)GT.1943-5606.0002737.

García-Gutiérrez, M., Cormenzana, J.L., Missana, T., Mingarro, M., 2004. Diffusion coefficients and accessible porosity for HTO and ^{36}Cl in compacted FEBEX bentonite. Appl. Clay Sci. 26 (1–4), 65–73. https://doi.org/10.1016/j.clay.2003.09.012.

Gates, W.P., Shaheen, U., Turney, T.W., Patti, A.F., 2016. Cyclic carbonate-sodium smectite intercalates. Appl. Clay Sci. 124-125, 94–101. https://doi.org/10.1016/j.clay.2016.02.005.

Gens, A., Sánchez, M., Guimarães, L.D.N., Alonso, E.E., Lloret, A., Olivella, S., Villar, M. V., Huertas, F., 2009. A full-scale in situ heating test for high-level nuclear waste disposal: Observations, analysis and interpretation. Géotechnique 59 (4), 377–399. https://doi.org/10.1680/geot.2009.59.4.377.

Glaus, M.A., Baeyens, B., Bradbury, M.H., Jakob, A., Van Loon, L.R., Yaroshchuk, A., 2007. Diffusion of ^{22}Na and ^{85}Sr in montmorillonite: evidence of interlayer diffusion being the dominant pathway at high compaction. Environ. Sci. Technol. 41 (2), 478–485. https://doi.org/10.1021/es061908d.

Gleason, M.H., Daniel, D.E., Eykholt, G.R., 1997. Calcium and sodium bentonite for hydraulic containment applications. J. Geotech. Geoenviron. Eng. 123 (5), 438–445. https://doi.org/10.1061/(ASCE)1090-0241(1997)123:5(438).

Grim, R.E., 1962. Applied Clay Mineralogy. McGraw–Hill.

Guarena, N., Dominijanni, A., Manassero, M., 2020. From the design of bottom landfill liner systems to the impact assessment of contaminants on underlying aquifers. Innov. Infrastruct. Solut. 5 (1), 2. https://doi.org/10.1007/s41062-019-0251-y.

Guarena, N., Dominijanni, A., Manassero, M., 2022. The role of diffusion induced electro-osmosis in the coupling between hydraulic and ionic fluxes through semipermeable clay soils. Soils Found. 62 (4), 101177 https://doi.org/10.1016/j.sandf.2022.101177.

Güven, N., 1992. Molecular aspects of clay-water interactions. In: Güven, N., Pollastro, R. M. (Eds.), Clay-Water Interface and its Rheological Implications: Workshop Lectures, vol. 4. The Clay Minerals Society, pp. 2–79.

Guyonnet, D., Gaucher, E., Gaboriau, H., Pons, C.H., Clinard, C., Norotte, V., Didier, G., 2005. Geosynthetic clay liner interaction with leachate: Correlation between permeability, microstructure, and surface chemistry. J. Geotech. Geoenviron. Eng. 131 (6), 740–749. https://doi.org/10.1061/(ASCE)1090-0241(2005)131:6(740).

Higashitani, K., Tanaka, T., Matsuno, Y., 1978. A kinematic interpretation on coagulation mechanism of hydrophobic colloids. J. Colloid Interface Sci. 63 (3), 551–560. https://doi.org/10.1016/S0021-9797(78)80014-9.

Holmboe, M., Wold, S., Jonsson, M., 2012. Porosity investigation of compacted bentonite using XRD profile modeling. J. Contam. Hydrol. 128 (1–4), 19–32. https://doi.org/10.1016/j.jconhyd.2011.10.005.

Hueckel, T., Loret, B., Gajo, A., 2002. Expansive clays as two-phase, deformable, reactive continua: Concepts and modeling options. In: Di Maio, C., Hueckel, T., Loret, B. (Eds.), Chemo-Mechanical Coupling in Clays: From Nano-Scale to Engineering Applications. Balkema, pp. 105–120.

Järvinen, J., Matusewicz, M., Itälä, A., 2016. Methodology for studying the composition of non-interlamellar pore water in compacted bentonite. Clay Miner. 51 (2), 173–187. https://doi.org/10.1180/claymin.2016.051.2.05.

Jo, H.Y., Katsumi, T., Benson, C.H., Edil, T.B., 2001. Hydraulic conductivity and swelling of nonprehydated GCLs permeated with single-species salt solutions. J. Geoetch. Geoenvrion. Eng. 127 (7), 557–567. https://doi.org/10.1061/(ASCE)1090-0241(2001)127:7(557).

Jo, H.Y., Benson, C.H., Edil, T.B., 2004. Hydraulic conductivity and cation exchange in non-prehydrated and prehydrated bentonite permeated with weak inorganic salt solutions. Clay Clay Miner. 52 (6), 661–679. https://doi.org/10.1346/CCMN.2004.0520601.

Jo, H.Y., Benson, C.H., Shackelford, C.D., Lee, J.M., Edil, T.B., 2005. Long-term hydraulic conductivity of a geosynthetic clay liner permeated with inorganic salt solutions. J. Geotech. Geoenviron. Eng. 131 (4), 405–417. https://doi.org/10.1061/(ASCE)1090-0241(2005)131:4(405).

Kang, J.B., Shackelford, C.D., 2009. Clay membrane testing using a flexible-wall cell under closed-system boundary conditions. Appl. Clay Sci. 44 (1–2), 43–58. https://doi.org/10.1016/j.clay.2009.01.006.

Katsumi, T., Ishimori, H., Ogawa, A., Yoshikawa, K., Hanamoto, K., Fukagawa, R., 2007. Hydraulic conductivity of nonprehydrated geosynthetic clay liners permeated with inorganic solutions and waste leachates. Soils Found. 47 (1), 79–96. https://doi.org/10.3208/sandf.47.79.

Katsumi, T., Ishimori, H., Onikata, M., Fukagawa, R., 2008. Long-term barrier performance of modified materials against sodium and calcium permeant solutions. Geotext. Geomembr. 26 (1), 14–30. https://doi.org/10.1016/j.geotexmem.2007.04.003.

Kolstad, D.C., Benson, C.H., Edil, T.B., 2004a. Hydraulic conductivity and swell of nonprehydrated geosynthetic clay liners permeated with multispecies inorganic solutions. J. Geotech. Geoenviron. Eng. 130 (12), 1236–1249. https://doi.org/10.1061/(ASCE)1090-0241(2004)130:12(1236).

Kolstad, D.C., Benson, C.H., Edil, T.B., Jo, H.Y., 2004b. Hydraulic conductivity of a dense prehydrated GCL permeated with aggressive inorganic solutions. Geosynth. Int. 11 (3), 233–241. https://doi.org/10.1680/gein.2004.11.3.233.

Komine, H., Ogata, N., 1999. Experimental study on swelling characteristics of sand-bentonite mixture for nuclear waste disposal. Soils Found. 39 (2), 83–97. https://doi.org/10.3208/sandf.39.2_83.

Kondo, M. (1996). *Method of activation of clay and activated clay* (U.S. Patent No. 5,573,583). U.S. Patent and Trademark Office.

Kozaki, T., Sato, H., Fujishima, A., Saito, N., Sato, S., Ohashi, H., 1996. Effect of dry density on activation energy for diffusion of strontium in compacted sodium montmorillonite. In: Gray, W.J., Traiy, I.R. (Eds.), MRS Online Proceedings Library, Vol. 465: Symposium II - Scientific Basis for Nuclear Waste Management XX. Springer, pp. 893–900.

Lagaly, G., 2006. Colloid clay science. In: Bergaya, F., Theng, B.K.G., Lagaly, G. (Eds.), Developments in Clay Science, Vol. 1: Handbook of Clay Science. Elsevier, pp. 141–245.

Laird, D.A., 1996. Model for crystalline swelling of 2:1 phyllosilicates. Clay Clay Miner. 44 (4), 553–559. https://doi.org/10.1346/CCMN.1996.0440415.

Laird, D.A., 2006. Influence of layer charge on swelling of smectites. Appl. Clay Sci. 34 (1–4), 74–87. https://doi.org/10.1016/j.clay.2006.01.009.

Leroy, P., Tournassat, C., Bernard, O., Devau, N., Azaroual, M., 2015. The electrophoretic mobility of montmorillonite. Zeta potential and surface conductivity effects. J. Colloid Interface Sci. 451, 21–39. https://doi.org/10.1016/j.jcis.2015.03.047.

Li, Q., Chen, J., Benson, C.H., Peng, D., 2021. Hydraulic conductivity of bentonite-polymer composite geosynthetic clay liners permeated with bauxite liquor. Geotext. Geomembr. 49 (2), 420–429. https://doi.org/10.1016/j.geotexmem.2020.10.015.

Li, D., Zainab, B., Tian, K., 2024. Effect of effective stress on hydraulic conductivity of bentonite–polymer geosynthetic clay liners to coal combustion product leachates. Environ. Geotech. https://doi.org/10.1680/jenge.21.00077 (in press).

Liu, Y., Gates, W.P., Bouazza, A., 2019. Impact of acid leachates on microtexture of bentonites used in geosynthetic clay liners. Geosynth. Int. 26 (2), 136–145. https://doi.org/10.1680/jgein.18.00043.

Luckham, P.F., Rossi, S., 1999. The colloidal and rheological properties of bentonite suspensions. Adv. Colloid Interf. Sci. 82 (1–3), 43–92. https://doi.org/10.1016/S0001-8686(99)00005-6.

Lyklema, J., Rovillard, S., De Coninck, J., 1998. Electrokinetics: the properties of the stagnant layer unraveled. Langmuir 14 (20), 5659–5663. https://doi.org/10.1021/la980399t.

Malusis, M.A., Daniyarov, A.S., 2016. Membrane efficiency and diffusive tortuosity of a dense prehydrated geosynthetic clay liner. Geotext. Geomembr. 44 (5), 719–730. https://doi.org/10.1016/j.geotexmem.2016.05.006.

Malusis, M.A., McKeehan, M.D., 2013. Chemical compatibility of model soil-bentonite backfill containing multiswellable bentonite. J. Geotech. Geoenviron. Eng. 139 (2), 189–198. https://doi.org/10.1061/(ASCE)GT.1943-5606.0000729.

Malusis, M.A., Shackelford, C.D., 2002. Coupling effects during steady-state solute diffusion through a semipermeable clay membrane. Environ. Sci. Technol. 36 (6), 1312–1319. https://doi.org/10.1021/es011130q.

Malusis, M.A., Shackelford, C.D., Olsen, H.W., 2001. A laboratory apparatus to measure chemico-osmotic efficiency coefficients for clay soils. Geotech. Test. J. 24 (3), 229–242. https://doi.org/10.1520/GTJ11343J.

Malusis, M.A., Maneval, J.E., Barben, E.J., Shackelford, C.D., Daniels, E.R., 2010. Influence of adsorption on phenol transport through soil–bentonite vertical barriers amended with activated carbon. J. Contam. Hydrol. 116 (1–4), 58–72. https://doi.org/10.1016/j.jconhyd.2010.06.001.

Malusis, M.A., Shackelford, C.D., Maneval, J.E., 2012. Critical review of coupled flux formulations for clay membranes based on nonequilibrium thermodynamics. J. Contam. Hydrol. 138-139, 40–59. https://doi.org/10.1016/j.jconhyd.2012.06.003.

Malusis, M.A., Kang, J.B., Shackelford, C.D., 2015. Restricted salt diffusion in a geosynthetic clay liner. Environ. Geotech. 2 (2), 68–77. https://doi.org/10.1680/envgeo.13.00080.

Malusis, M.A., Dominijanni, A., Scalia, J., Guarena, N., Sample-Lord, K.M., Bohnhoff, G. L., Shackelford, C.D., Manassero, M., 2021. Assessing the influence of chemico-osmosis on solute transport in bentonite membranes based on combined phenomenological and physical modeling. Jpn. Geotech. Soc. Spec. Publ. 9 (2), 37–44. https://doi.org/10.3208/jgssp.v09.cpeg023.

Manassero, M., 2020. Second ISSMGE R. Kerry Rowe Lecture: on the intrinsic, state, and fabric parameters of active clays for contaminant control. Can. Geotech. J. 57 (3), 311–336. https://doi.org/10.1139/cgj-2019-0033.

Manassero, M., Dominijanni, A., 2003. Modelling the osmosis effect on solute migration through porous media. Géotechnique 53 (5), 481–492. https://doi.org/10.1680/geot.2003.53.5.481.

Manassero, M., Fratalocchi, E., Pasqualini, E., Spanna, C., Verga, F., 1995. Containment with vertical cutoff walls. In: Acar, Y.B., Daniel, D.E. (Eds.), Proceedings of Geoenvironment 2000: Characterization, Containment, Remediation, and Performance in Environmental Geotechnics, vol. 2. American Society of Civil Engineers, pp. 1142–1172.

Manassero, M., Benson, C.H., Bouazza, A., 2000. Solid waste containment systems. In: Proceedings of GeoEng2000: An International Conference on Geotechnical and Geological Engineering, vol. 1. Technomic Publishing Co, pp. 520–642.

Manassero, M., Dominijanni, A., Guarena, N., 2018. Modelling hydro-chemo-mechanical behaviour of active clays through the fabric boundary surface. In: Wu, W., Yu, H.S. (Eds.), Proceedings of China-Europe Conference on Geotechnical Engineering, vol. 2. Springer, pp. 1618–1626.

Matusewicz, M., Pirkkalainen, K., Liljeström, V., Suuronen, J.P., Root, A., Muurinen, A., Serimaa, R., Olin, M., 2013. Microstructural investigation of calcium montmorillonite. Clay Miner. 48 (2), 267–276. https://doi.org/10.1180/claymin.2013.048.2.08.

Mazzieri, F., Bernardo, D., 2024. Permeability and solute sorption of unamended and polymer-enhanced geosynthetic clay liners. Environ. Geotech. https://doi.org/10.1680/jenge.21.00124 (in press).

Mazzieri, F., Di Emidio, G., 2015. Hydraulic conductivity of a dense prehydrated geosynthetic clay liner. Geosynth. Int. 22 (1), 138–148. https://doi.org/10.1680/gein.14.00037.

Mazzieri, F., Di Emidio, G., Van Impe, P.O., 2010. Diffusion of calcium chloride in a modified bentonite: impact on osmotic efficiency and hydraulic conductivity. Clay Clay Miner. 58 (3), 351–363. https://doi.org/10.1346/CCMN.2010.0580306.

Mazzieri, F., Di Emidio, G., Fratalocchi, E., Di Sante, M., Pasqualini, E., 2013. Permeation of two GCLs with an acidic metal-rich synthetic leachate. Geotext. Geomembr. 40, 1–11. https://doi.org/10.1016/j.geotexmem.2013.07.011.

Mazzieri, F., Di Emidio, G., Pasqualini, E., 2017. Effect of wet-and-dry ageing in seawater on the swelling properties and hydraulic conductivity of two amended bentonites. Appl. Clay Sci. 142 (6), 40–51. https://doi.org/10.1016/j.clay.2016.10.031.

Mesri, G., Olson, R.E., 1971. Mechanisms controlling the permeability of clays. Clay Clay Miner. 19 (3), 151–158. https://doi.org/10.1346/CCMN.1971.0190303.

Missana, T., García-Gutiérrez, M., 2007. Adsorption of bivalent ions (Ca(II), Sr(II) and Co (II)) onto FEBEX bentonite. Phys. Chem. Earth Parts A/B/C 32 (8–14), 559–567. https://doi.org/10.1016/j.pce.2006.02.052.

Mitchell, J.K., Soga, K., 2005. Fundamentals of Soil Behavior (3rd Edition). Wiley.

Moore, D.M., Reynolds, R.C., 1997. X-Ray Diffraction and the Identification and Analysis of Clay Minerals (2nd Edition). Oxford University Press.

Musso, G., Cosentini, R.M., Dominijanni, A., Guarena, N., Manassero, M., 2017. Laboratory characterization of the chemo-hydro-mechanical behaviour of chemically sensitive clays. Riv. Ital. Geotech. 51 (3), 22–47. https://doi.org/10.19199/2017.3.0557-1405.022.

Muurinen, A., Karnland, O., Lehikoinen, J., 2004. Ion concentration caused by an external solution into the porewater of compacted bentonite. Phys. Chem. Earth Parts A/B/C 29 (1), 119–127. https://doi.org/10.1016/j.pce.2003.11.004.

Muurinen, A., Carlsson, T., Root, A., 2013. Bentonite pore distribution based on SAXS, chloride exclusion and NMR studies. Clay Miner. 48 (2), 251–266. https://doi.org/10.1180/claymin.2013.048.2.07.

Ni, H., Shen, S.Q., Fu, X.L., Wang, C.M., Du, Y.J., 2022. Assessment of membrane and diffusion behavior of soil-bentonite slurry trench wall backfill consisted of sand and Xanthan gum amended bentonite. J. Clean. Prod. 365, 132779 https://doi.org/10.1016/j.jclepro.2022.132779.

Norris, A., 2021. Mechanisms of interaction between montmorillonite and anionic polymer amendments in geosynthetic clay liners [Doctoral dissertation, Colorado State University]. Colorado State University Theses and Dissertations Archive. https://hdl.handle.net/10217/100532.

Norris, A., Aghazamani, N., Scalia, J., Shackelford, C.D., 2022. Hydraulic performance of geosynthetic clay liners comprising anionic polymer-enhanced bentonites. J. Geotech. Geoenviron. Eng. 148 (6), 04022039. https://doi.org/10.1061/(ASCE)GT.1943-5606.0002781.

Norris, A., Scalia, J., Shackelford, C.D., 2023. Mechanisms controlling the hydraulic conductivity of anionic polymer-enhanced GCLs. Geosynth. Int. 30 (6), 628–650. https://doi.org/10.1680/jgein.21.00051.

Norrish, K., Quirk, J.P., 1954. Crystalline swelling of montmorillonite: use of electrolytes to control swelling. Nature 173 (4397), 255–256. https://doi.org/10.1038/173255a0.

Novich, B.E., Ring, T.A., 1984. Colloid stability of clays using photon correlation spectroscopy. Clay Clay Miner. 32 (5), 400–406. https://doi.org/10.1346/CCMN.1984.0320508.

Olsen, S.R., Kemper, W.E., 1968. Movement of nutrients to plant roots. Adv. Agron. 20, 91–151. https://doi.org/10.1016/S0065-2113(08)60855-X.

Onikata, M., Kondo, M., Kamon, M., 1996. Development and characterization of a multiswellable bentonite. In: Kamon, M. (Ed.), Proceedings of the 2nd International Congress on Environmental Geotechnics, vol. 1. CRC Press/Balkema, pp. 587–590.

Onikata, M., Kondo, M., Hayashi, N., Yamanaka, S., 1999. Complex formation of cation-exchanged montmorillonites with propylene carbonate: osmotic swelling in aqueous electrolyte solutions. Clay Clay Miner. 47 (5), 672–677. https://doi.org/10.1346/CCMN.1999.0470514.

Oscarson, D.W., 1994. Surface diffusion: is it an important transport mechanism in compacted clays? Clay Clay Miner. 42 (5), 534–543. https://doi.org/10.1346/CCMN.1994.0420504.

Overbeek, J.T.G., 1982. Strong and weak points in the interpretation of colloid stability. Adv. Colloid Interf. Sci. 16 (1), 17–30. https://doi.org/10.1016/0001-8686(82)85003-3.

Petrov, R.J., Rowe, R.K., 1997. Geosynthetic clay liner (GCL) – chemical compatibility by hydraulic conductivity testing and factors impacting its performance. Can. Geotech. J. 34 (6), 863–885. https://doi.org/10.1139/t97-055.

Prongmanee, N., Chai, J.C., Shen, S., 2018. Hydraulic properties of polymerized bentonites. J. Mater. Civ. Eng. 30 (10), 04018247. https://doi.org/10.1061/(ASCE)MT.1943-5533.0002442.

Puma, S., Dominijanni, A., Manassero, M., Zaninetta, L., 2015. The role of physical pretreatments on the hydraulic conductivity of natural sodium bentonites. Geotext. Geomembr. 43 (3), 263–271. https://doi.org/10.1016/j.geotexmem.2015.02.001.

Qiu, H., Yu, J., 2008. Polyacrilate/carboxymethylcellulose modified montmorillonite superabsorbent nanocomposite: Preparation and water absorbency. J. Appl. Polym. Sci. 107 (1), 118–123. https://doi.org/10.1002/app.26261.

Rowe, R.K., 1998. Geosynthetics and the minimization of contaminant migration through barrier systems beneath solid waste. In: Rowe, R.K. (Ed.), Proceedings of the 6th International Conference on Geosynthetics, vol. 1. Industrial Fabrics Association International, pp. 27–103.

Rowe, R.K., 2014. Performance of GCLs in liners for landfill and mining applications. Environ. Geotech. 1 (1), 3–21. https://doi.org/10.1680/envgeo.13.00031.

Saiyouri, N., Tessier, D., Hicher, P.Y., 2004. Experimental study of swelling in unsaturated compacted clays. Clay Miner. 39 (4), 469–479. https://doi.org/10.1180/0009855043940148.

Santamarina, J.C., Klein, K., Palomino, A., Guimaraes, M.S., 2002. Micro-scale aspects of chemical-mechanical coupling: Interparticle forces and fabric. In: Di Maio, C., Hueckel, T., Loret, B. (Eds.), Chemo-Mechanical Coupling in Clays: From Nano-Scale to Engineering Applications. Balkema, pp. 47–64.

Scalia, J., 2012. Bentonite-polymer composites for containment applications [Doctoral dissertation, University of Wisconsin-Madison]. ProQuest Dissertations & Theses Global. https://digital.library.wisc.edu/1711.web/proquest-digital-dissertations.

Scalia, J., Benson, C.H., 2017. Polymer fouling and hydraulic conductivity of mixtures of sodium bentonite and a bentonite-polymer composite. J. Geotech. Geoenviron. Eng. 143 (4), 04016112. https://doi.org/10.1061/(ASCE)GT.1943-5606.0001628.

Scalia, J., Benson, C.H., Bohnhoff, G.L., Edil, T.B., Shackelford, C.D., 2014. Long-term hydraulic conductivity of a bentonite-polymer composite permeated with aggressive inorganic solutions. J. Geotech. Geoenviron. Eng. 140 (3), 04013025. https://doi.org/10.1061/(ASCE)GT.1943-5606.0001040.

Scalia, J., Bohnhoff, G.L., Shackelford, C.D., Benson, C.H., Sample-Lord, K.M., Malusis, M.A., Likos, W.J., 2018. Enhanced bentonites for containment of inorganic waste leachates by GCLs. Geosynth. Int. 25 (4), 392–411. https://doi.org/10.1680/jgein.18.00024.

Schlögl, R., 1955. Zur theorie der anomalen osmose. Z. Phys. Chem. 3, 73–102. https://doi.org/10.1524/zpch.1955.3.1_2.073.

Schmid, G., 1950. Zur elektrochemie feinporiger kapillarsysteme I. Übersicht. Z. Elektrochem. Angew. Phys. Chem. 54 (6), 424–430. https://doi.org/10.1002/bbpc.19500540610.

Segad, M., Jönsson, B., Cabane, B., 2012a. Tactoid formation in montmorillonite. J. Phys. Chem. C 116 (48), 25425–25433. https://doi.org/10.1021/jp3094929.

Segad, M., Hanski, S., Olsson, U., Ruokolainen, J., Åkesson, T., Jönsson, B., 2012b. Microstructural and swelling properties of Ca and Na montmorillonite: (in situ) Observations with cryo-TEM and SAXS. J. Phys. Chem. C 116 (13), 7596–7601. https://doi.org/10.1021/jp300531y.

Shackelford, C.D., 1991. Laboratory diffusion testing for waste disposal – a review. J. Contam. Hydrol. 7 (3), 177–217. https://doi.org/10.1016/0169-7722(91)90028-Y.

Shackelford, C.D., 2013. Membrane behavior in engineered bentonite-based containment barriers: State of the art. In: Manassero, M., Dominijanni, A., Foti, S., Musso, G. (Eds.), Proceedings of the International Symposium on Coupled Phenomena in Environmental Geotechnics. CRC Press/Balkema, pp. 45–60. https://doi.org/10.1201/b15004-7.

Shackelford, C.D., Daniel, D.E., 1991. Diffusion in saturated soil: I. Background. J. Geotech. Eng. 117 (3), 467–484. https://doi.org/10.1061/(ASCE)0733-9410(1991)117:3(467).

Shackelford, C.D., Lee, J.M., 2003. The destructive role of diffusion on clay membrane behavior. Clay Clay Miner. 51 (2), 186–196. https://doi.org/10.1346/CCMN.2003.0510209.
Shackelford, C.D., Moore, S.M., 2013. Fickian diffusion of radionuclides for engineered containment barriers: diffusion coefficients, porosities, and complicating issues. Eng. Geol. 152 (1), 133–147. https://doi.org/10.1016/j.enggeo.2012.10.014.
Shackelford, C.D., Benson, C.H., Katsumi, T., Edil, T.B., Lin, L., 2000. Evaluating the hydraulic conductivity of GCLs permeated with non-standard liquids. Geotext. Geomembr. 18 (2–4), 133–161. https://doi.org/10.1016/S0266-1144(99)00024-2.
Shackelford, C.D., Sevick, G.W., Eykholt, G.R., 2010. Hydraulic conductivity of geosynthetic clay liners to tailings impoundment solutions. Geotext. Geomembr. 28 (2), 149–162. https://doi.org/10.1016/j.geotexmem.2009.10.005.
Shackelford, C.D., Lu, N., Malusis, M.A., Sample-Lord, K.M., 2019. Research challenges involving coupled flows in geotechnical engineering. In: Lu, N., Mitchell, J.K. (Eds.), Geotechnical Fundamentals for Addressing New World Challenges. Springer, pp. 237–274.
Shang, J.Q., Lo, K.Y., Quigley, R.M., 1994. Quantitative determination of potential distribution in Stern-Gouy double-layer model. Can. Geotech. J. 31 (5), 624–636. https://doi.org/10.1139/t94-075.
Soga, K., Joshi, K., Evans, J.C., 2013. Cement bentonite cutoff walls for polluted sites. In: Manassero, M., Dominijanni, A., Foti, S., Musso, G. (Eds.), Proceedings of the International Symposium on Coupled Phenomena in Environmental Geotechnics. CRC Press/Balkema, pp. 149–165. https://doi.org/10.1201/b15004-15.
Spielman, L.A., 1970. Viscous interactions in Brownian coagulation. J. Colloid Interface Sci. 33 (4), 562–571. https://doi.org/10.1016/0021-9797(70)90008-1.
Sposito, G., 2008. The Chemistry of Soils (2nd Edition). Oxford University Press.
Tian, K., Likos, W.J., Benson, C.H., 2016. Pore-scale imaging of polymer-modified bentonite in saline solutions. In: Zekkos, D., Farid, A., De, A., Reddy, K.R., Yesiller, N. (Eds.), Geo-Chicago 2016: Sustainability and Resiliency in Geotechnical Engineering. American Society of Civil Engineers, pp. 468–477.
Tian, K., Likos, W.J., Benson, C.H., 2019. Polymer elution and hydraulic conductivity of bentonite-polymer composite geosynthetic clay liners. J. Geotech. Geoenviron. Eng. 145 (10), 04019071. https://doi.org/10.1061/(ASCE)GT.1943-5606.0002097.
Tong, S., Sample-Lord, K.M., 2022. Coupled solute transport through a polymer-enhanced bentonite. Soils Found. 62 (6), 101235 https://doi.org/10.1016/j.sandf.2022.101235.
Tong, S., Sample-Lord, K.M., Bohnhoff, G.L., 2021. Diffusion through sodium and polymer enhanced bentonites exposed to dilute and aggressive solutions. Can. Geotech. J. 58 (5), 603–618. https://doi.org/10.1139/cgj-2019-0809.
Tournassat, C., Appelo, C.A.J., 2011. Modelling approaches for anion exclusion in compacted Na-bentonite. Geochim. Cosmochim. Acta 75 (13), 3698–3710. https://doi.org/10.1016/j.gca.2011.04.001.
Trauger, R., Darlington, J., 2000. Next-Generation Geosynthetic Clay Liners for Improved Durability and Performance (TR-220). Colloidal Environmental Technologies Company.
van Olphen, H., 1977. An Introduction to Clay Colloid Chemistry (2nd Edition). Wiley.
Verburg, K., Baveye, P., 1994. Hysteresis in the binary exchange of cations on 2:1 clay minerals: a critical review. Clay Clay Miner. 42 (2), 207–220. https://doi.org/10.1346/CCMN.1994.0420211.
Verwey, E.J.W., Overbeek, J.T.G., 1948. Theory of the Stability of Lyophobic Colloids. Elsevier.
Villar, M.V., Iglesias, R.J., García-Siñeriz, J.L., 2020. State of the in situ Febex test (GTS, Switzerland) after 18 years: a heterogeneous bentonite barrier. Environ. Geotech. 7 (2), 147–159. https://doi.org/10.1680/jenge.17.00093.
Yaroshchuk, A.E., 1995. Osmosis and reverse osmosis in fine-porous charged diaphragms and membranes. Adv. Colloid Interf. Sci. 60 (1–2), 1–93. https://doi.org/10.1016/0001-8686(95)00246-M.
Yeung, A.T., Mitchell, J.K., 1993. Coupled fluid, electrical and chemical flows in soil. Géotechnique 43 (1), 121–134. https://doi.org/10.1680/geot.1993.43.1.121.
Zainab, B., Wireko, C., Li, D., Tian, K., Abichou, T., 2021. Hydraulic conductivity of bentonite-polymer geosynthetic clay liners to coal combustion product leachates. Geotext. Geomembr. 49 (5), 1129–1138. https://doi.org/10.1016/j.geotexmem.2021.03.007.